DELTA-ELECTRON EMISSION

IN 10 MeV F^{q+} + Ne (q = 6,8,9)

by

ALEXANDER ERICH SKUTLARTZ

Staatsexamen, Universitaet Freiburg, West Germany, 1980

A MASTER'S THESIS

submitted in partial fulfillment of the

requirements for the degree

MASTER OF SCIENCE

Department of Physics

KANSAS STATE UNIVERSITY

Manhattan, Kansas

1983

Approved by:

S. Hagmann

Major Professor

TABLE OF CONTENTS

Chapter | Page

LIST OF TABLES

LIST OF FIGURES

Figure		Page

ACKNOWLEDGEMENTS

I would like to thank my major professor, Siegbert Hagmann, for his guidance and help in all phases of this thesis.

I would like to express my appreciation to the members of my committee, P. Richard and C. L. Cocke, for their interest in this work and for many helpful discussions.

I would like to thank my parents for their love, support and encouragement, which made my stay at this institution possible.

Special thanks go to Ivette for her love, care and understanding, which made the work on this thesis more bearable.

I also would like to thank H. Schmidt-Boecking and R. Schuch for making available the use of the Parallel-Plate-Avalanche detector and its supporting electronics, and D. Trautmann for carrying out the theoretical calculations presented in this thesis.

I appreciate the expert typing of this thesis by KoKo Himes.

The financial support by the U.S. Department of Energy under contract No. De-AC02-76ER0753-1302 is gratefully acknowledged.

Chapter 1

INTRODUCTION

During the last decade a large number of experiments have been undertaken to investigate the emission of delta-electrons, i.e. electrons ejected in the primary collision process in ion-atom collisions.[1-12,36] These electrons, emitted from a specific atomic state, often provide a more direct insight into the collision mechanisms and atomic structures involved than the observation of secondary decay products (photons, Auger-electrons) from the ionized target.

Mostly total, singly and doubly differential cross sections as a function of delta-electron energy and emission angle for proton impact in gaseous targets have been obtained.[1-7,10,12,36] Few results for heavier projectiles are known.[8,9,11]

A mechanism responsible for the production of delta-electrons is the direct Coulomb ionization. When a charged particle (ion) passes through or near an atom, the most prominant interaction is the Coulomb attraction between the ion and the orbital electrons of the target atom. This interaction causes the electrons to be "pulled out" of the atom provided the energy given to it is enough to raise it from its binding in the potential well of the target nucleus to the continuum. Since the Coulomb interaction is well understood, these experiments provide useful information availabe for comparison with various theoretical models. However, since only cross sections and differential cross sections for delta-electron production have been reported on, only information on the final result of such an ionization event can be extracted, knowledge about the kinematics of the ionization process itself can not be easily deduced.

Only recently results became available that have been obtained by applying stricter conditions on the experimental collision system. Winter and Schuch[10] reported on the energy distribution of delta-electrons from the Argon-K-shell following proton impact, and Cocke et al.[11] for the first time measured the impact parameter dependence of delta-electrons in Sulfur-Argon collisions. While both experiments require the use of coincidence techniques, the latter is of special interest, since fixing the impact parameter allows one to determine the momentum carried into the collision by the projectile and thus provides an important piece of information about the kinematics of the ionization process itself. Alas, Cocke et al. used S^{5+} and S^{11+} as projectiles and thus electrons were carried into the collision and no distinction between target and projectile electrons could be made in the specta obtained. An application of the results to theoretical calculations proved difficult under these conditions.

The purpose of the experiment presented here was to gain more information about the ionization process in heavy ion collisions by determining the delta-electron emission probability per collision as a function of the impact parameter, the electron energy and the electron emission angle. To eliminate the occurrence of projectile electrons, bare F^{9+} ions impinging on a Neon gas target were used as the system to be investigated. For comparison collisions of hydrogen- and lithium-like Fluorine ions were also examined. The delta-electrons were recorded in coincidence with the scattered projectiles.

In Chapter 2 of the present work, an outline of the main theoretical models describing direct Coulomb ionization will be given. Chapter 3 contains an introduction to the principles of coincidence techniques.

A description of the apparatus used and the experimental procedure will follow in Chapter 4. Chapter 5 is designed to present experimental results and a comparison with a theoretical model calculation. These results will be discussed in Chapter 6 and possible conclusions will be drawn.

Chapter 2

THEORETICAL BACKGROUND

In this section a brief outline of the main three theoretical models dealing with direct Coulomb ionization and applicable to the experiment presented in this work will be given. The models are:

The Plane Wave Born Approximation (PWBA)

The Binary Encounter Approximation (BEA)

The Semiclassical Approximation (SCA).

In all three models the ionization process is treated as a direct Coulomb excitation of the target electron into the continuum and the projectile is assumed to have a point-like charge distribution. Coulomb excitation itself dominates at projectile velocities so high that the projectiles move as bare nuclei through the target. But even a slow projectile acts as a point charge as long as its K-shell radius $R_p = a_o/Z_p$ is large compared to the target K-shell radius $R_T = a_o/Z_T$. Thus, for K-shell Coulomb excitation the projectile can be treated as a point charge for all projectile velocities as long as the condition $Z_p < Z_T$ is satisfied,[13] and K-shell Coulomb excitation will be the dominant process.[14]

The most extensive theoretical calculations have been performed in the framework of the Plane Wave Born Approximation.[15-18] This model assumes that the projectile acts as a point charge, that the initial and final projectile waves are planar over all space and that the target electrons are in the states corresponding to those of an unperturbed target. The mechanism responsible for the direct ionization of a target electron is the interaction of the Coulomb field of the incoming ion and the bound electron in the target atom. The expression for the cross section in differential form is thus written in first order time-dependent perturbation theory as[19]

$$d\sigma_{if} = 16\pi Z_p^2 \cdot \left(\frac{e^2}{\hbar v_p}\right)^2 \cdot \frac{dk}{k^3} \left|\int e^{i\vec{k}\cdot\vec{r}}\ \psi_f^*(\vec{r})\psi_i(\vec{r})d^3r\right| \qquad (2.1)$$

where $\hbar\vec{k}$ is the momentum transferred for ionization into a given final state ψ_f. V_p is the velocity of the projectile and $\vec{r}$ is the coordinate of the electron relative to the target nucleus. To obtain the total cross section, one has to integrate the above expression over all momentum transfers compatible with the production of the final state and sum over all permissible final states (i.e. integrate over all allowable kinetic energies and directions of motion of the ejected electron). Often a further approximation is introduced by using appropriate hydrogenic wave functions for the initial state of the bound target electron.

In the Binary Encounter Approximation[19-21] the dominant interaction producing the transition is the direct energy transfer between the incident projectile and the bound electron. The role of the target nucleus reduces to simply providing the velocity distribution of the bound electron. The term binary encounter has its origin in viewing the process as a collision of the incident projectile with momentum $\vec{k}(P)$ with a free electron with momentum $\vec{k}(E)$. Since the classical and quantum mechanical cross sections for Coulomb scattering are identical, one uses a classical analysis to obtain a differential cross section $\frac{d\sigma}{d\Delta E}$, where ΔE is the energy exchange between projectile and electron. Then, one integrates over ΔE and averages over the velocity distribution $f(v)$ of the electron. Thus

$$\sigma(v_p) = N \cdot \int_{E_B}^{\infty} \sigma_i \cdot f(v)dv \qquad (2.2)$$

where

$$\sigma_i = \int_{E_B}^{E} \frac{d\sigma}{d\Delta E} \; d\Delta E$$

f(v) is the velocity (momentum) distribution of the target electron and N is the number of equivalent electrons having a binding energy E_B. The latter integration can be done in closed form, and by using isotropic hydrogenic velocity distributions for closed shells, one obtains[22]

$$\sigma = \frac{N Z_p^2 \sigma_o}{E_B^2} \cdot G(v) \tag{2.3}$$

where

$$v = \frac{v_p}{v_o} \; , \; v_o = \sqrt{\frac{2E_B}{M_o}} \; , \; \sigma_o = \pi e^2$$

and G(v) is a tabulated function of the scaled velocity.[21] McGuire[32] and McGuire and Richard[21] obtained an expression for σ as a function of the scattering probability in an impact parameter formulation of this theoretical model.

The basic assumptions in the Semiclassical Approximation[23-40] are, that the point-charge particle moves on a classical trajectory and that only one target electron is actively involved in the ionization process. If the electron system is presented by

$$H_{e\ell} \; \psi_k \; (\vec{r}_1, \ldots, \vec{r}_{Z_T}) = E_k \; \psi_k \; (\vec{r}_1, \ldots, \vec{r}_{Z_T}) \tag{2.4}$$

the perturbation by the point charge is given by

$$V(t) = -\sum_{n=1}^{Z_T} \frac{Z_p \cdot e^2}{|\vec{r}_n - \vec{R}(t)|} \tag{2.5}$$

where $\vec{R}(t)$ describes the trajectory of the projectile. Thus the excitation amplitude becomes in first order perturbation theory

$$a_{fi} = - i/\hbar \int_{-\infty}^{+\infty} e^{i(E_f - E_i)t/\hbar} < \psi_f \; |V(t)| \; \psi_i > dt \tag{2.6}$$

The ionization probability evolves from this as

$$P(b) = \int_0^{E_{MAX}} \frac{dP(b)}{dE_f}\, dE_f \qquad (2.7)$$

where

$$\frac{dP(b)}{dE_f} = |a_{E_f,i}\ (t\to\infty)|^2 \qquad (2.8)$$

and

$$a_{E_f,i} = -i/\hbar \int_{-\infty}^{+\infty} e^{i\omega t} < E_f\, |- \frac{Z_p \cdot e^2}{|\vec{r}-\vec{R}(t)|}\, |i > dt \qquad (2.9)$$

Here, $|E_f>$ is normalized to a delta-function in energy. Finally, one obtains the total cross section by

$$\sigma = 2\pi \int_0^{\infty} P(b) \cdot bdb \qquad (2.10)$$

In each of the above theoretical models the main assumption is $Z_p \ll Z_T$. However, in the experiment presented here, the system 10 MeV F^{9+} + Ne with Z_p/Z_T = .9 is near symmetric. Numerous additional assumptions and corrections have been introduced to extend the validity of these models into this near symmetric region. For all models these corrections are similar in character and will be discussed in more detail in the case of the Semiclassical Approximation in Chapter 5.

Chapter 3

PRINCIPLES OF COINCIDENT IMPACT PARAMETER MEASUREMENTS

3-1) Impact Parameter b and Scattering Angle

A classical scattering event between a projectile of nuclear charge Z_p and a target of nuclear charge Z_T is shown in Figure 1. The projectile trajectory will be described classically as long as its de Broglie wavelength λ ($\lambda = 29/\sqrt{m(\mathrm{amu})\cdot E(\mathrm{MeV})}$ fm) is small compared to the dimensions of the scattering center $r_n = n^2 \cdot a_o/Z_p$; e.g. for 10 MeV F + Ne, λ=2.10 fm, r_K=53 fm, r_L=212 fm). If the trajectory is described in such a way, a one-to-one relation between scattering angle θ and impact parameter b can be established, depending on a Coulombic internuclear potential. This relation is of importance, since the scattering angle, but not the impact parameter, can be determined experimentally. For a pure Coulombic internuclear potential this relation is given by

$$b = \frac{Z_p \cdot Z_T \cdot e^2}{2E_{CM} \cdot \tan \frac{\theta^{CM}}{2}} \qquad (3.1)$$

where E_{CM} is the center of mass energy and θ^{CM} is the center of mass scattering angle. However, for very small scattering angles, i.e. large impact parameters, Rutherford scattering is no longer valid, because the projectile does not see the total target nuclear charge, but a somewhat reduced value of Z_T due to the screening of the target electrons. An exponentially screened internuclear potential of the form

$$V = V_{Ruth} \cdot e^{-r/a} \qquad (3.2)$$

has to be applied. Using a computer code,[33] Hagmann et al.[34] determined

Figure 1. A diagram of a scattering event, characterized by the charge Z_p, mass m_p and velocity v_p of the projectile, the charge Z_T and mass m_T of the target, the impact parameter b, the scattering angle θ and the solid angle indicated by $d\theta$.

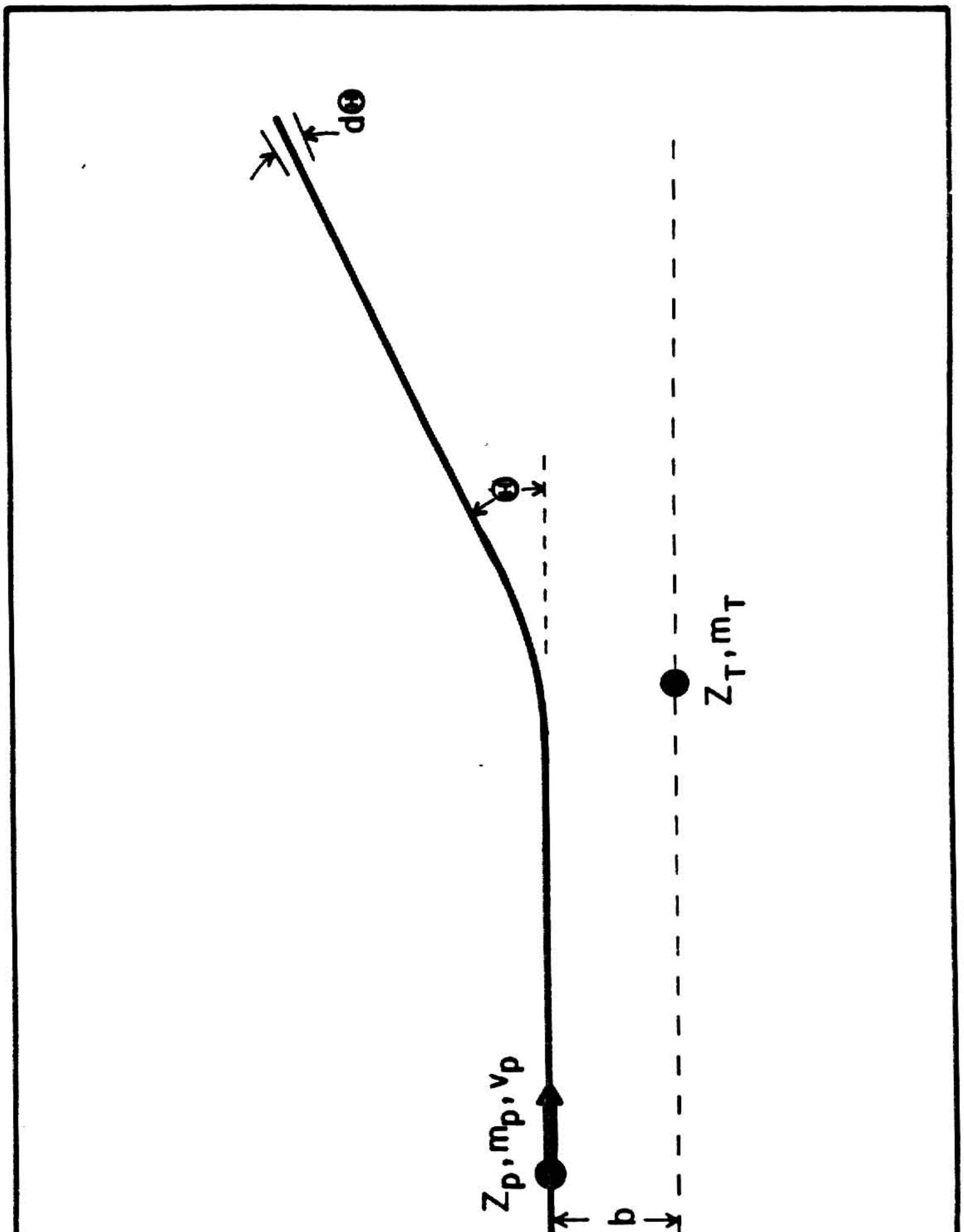
dΘ
Θ
Z_T, m_T
Z_p, m_p, v_p
b

the screening parameter a for the system 10 MeV F + Ne, which is investigated in this paper, to be a = .52 a.u. from an experimentally obtained scattering function. The relation between impact parameter b and laboratory scattering angle θ follows from this as shown in Figure 2.

3-2) Coincident Impact Parameter Measurements

To obtain experimentally the probability P(b) for the emission of an electron per collision event, one has to measure the rate of projectiles scattered into an angle θ and the rate of electrons emitted in the same collision process. Thus, the ionization probability as a function of the impact parameter b will be given by

$$P(b) = \frac{N_t}{N_p} \cdot \frac{1}{\varepsilon_e} \cdot \frac{1}{d\Omega_e} \tag{3.3}$$

where N_t is the number of true coincidences between the scattered projectiles and emitted electrons, N_p is the number of scattered projectiles into an angle θ and ε_e and $d\Omega_e$ are the efficiency and the solid angle subtended by the electron detection device. N_p is given by

$$N_p = i/q \, \frac{d\sigma_R}{d\Omega} \cdot \eta_T \cdot \varepsilon_p \cdot d\Omega_p \tag{3.4}$$

where i/q is the number of incoming projectiles per unit time, $\frac{d\sigma_R}{d\Omega}$ is the Rutherford scattering cross section, η_T is the target density and ε_p and $d\Omega_p$ are the efficiency and solid angle of the particle detector. The spectrum of time delays t between electron and scattered particle detection consists of two features: a background of random coincidences which occur when the electron and scattered particle have their origin not in the same collision event; and a peak of real coincidences centered about t_o. The time t_o contains the net delay of scattered particle detection, including the projectile's time of flight from the scattering center to the particle

Figure 2. The impact parameter b as a function of the laboratory scattering angle θ for a pure Coulombic (b_R) and a screened Coulombic (b_{sc}) internuclear interaction.

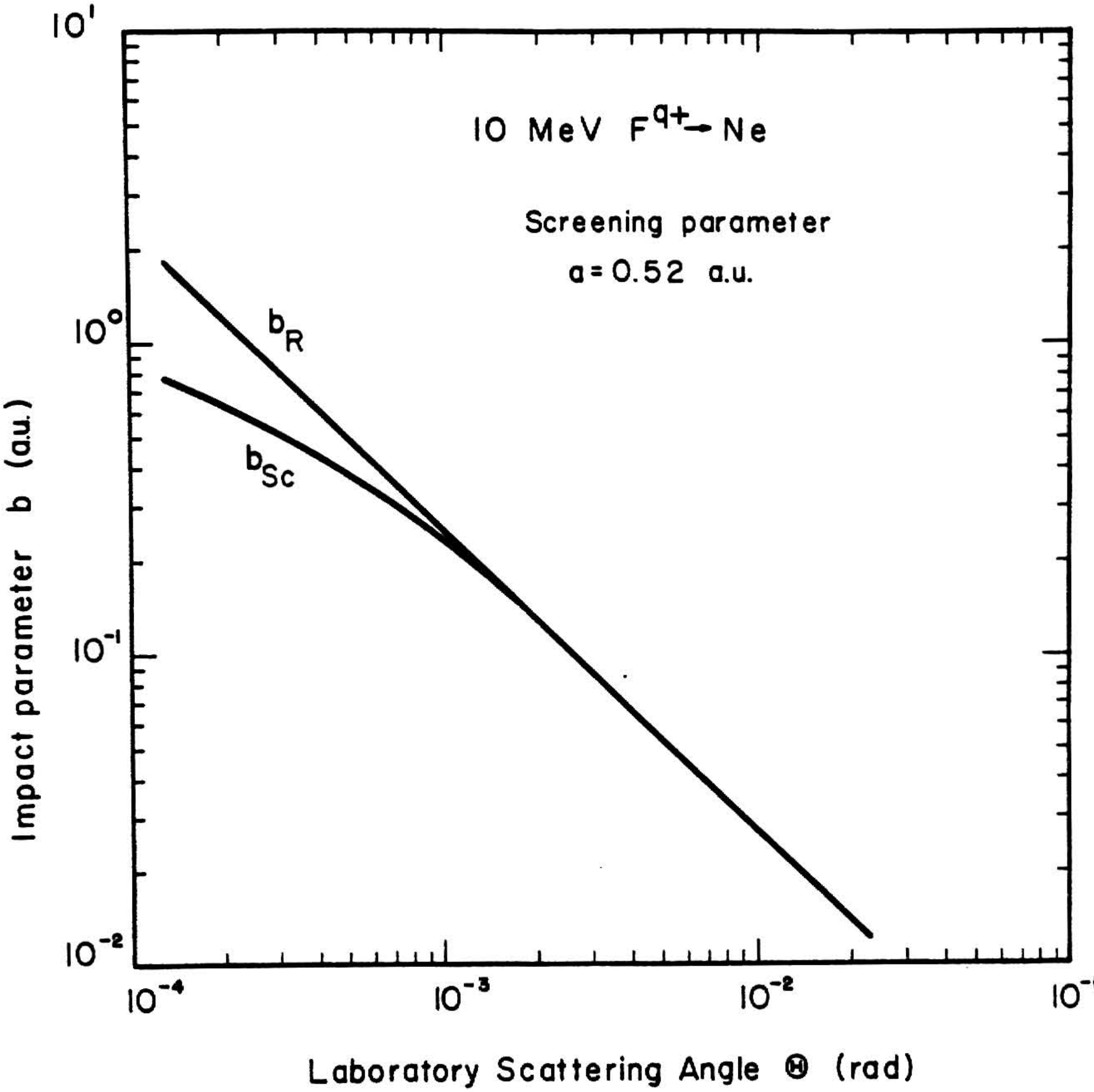

10 MeV $F^{q+} \rightarrow Ne$
Screening parameter
a = 0.52 a.u.
b_R
b_{Sc}
10^1
10^0
10^{-1}
10^{-2}
Impact parameter b (a.u.)
10^{-4}
10^{-3}
10^{-2}
10^{-1}
Laboratory Scattering Angle Θ (rad)

detector, the detector differential response time and electronic delays. The rate of random coincidences in each time channel of width Δt is given by[35]

$$N_r^{\Delta t} = N_p \cdot N_e^{sing} \cdot \Delta t \cdot e^{-tN_p} \qquad (3.5)$$

and the integrated count rate of true coincidences is

$$N_t = N_p \cdot P(b) \cdot \varepsilon_e \cdot d\Omega_e \cdot e^{-t_o N_p} \qquad (3.6)$$

where the single electron count rate is

$$N_e^{sing} = i/q \cdot \eta_T \cdot \sigma_i \cdot \varepsilon_e \cdot d\Omega_e \qquad (3.7)$$

with the ionization cross section σ_i for the target shell to be probed.

Normally, $N_e^{sing} \ll N_p$, thus one uses the electron detection signal as a starting measure to determine the time delay t, i.e. one feeds this signal as the "start signal" into a time-amplitude converter (TAC) and uses the scattered projectile detection signal as a "stop signal" to obtain a time delay spectrum (TAC spectrum). Unless N_p is very large, the products $t \cdot N_p$ and $t_o \cdot N_p$ will be small compared to unity (typically, t and t_o are in the nanosecond range, whereas N_p is of the order of some ten thousand counts per second) and the exponential factors in the above expressions (3.5) and (3.6) can be neglected. Using this, the ratio of real coincidences to randoms underlying the real peak is obtained to be

$$\frac{N_t}{N_r} = \frac{P(b)}{\sigma i} \cdot \frac{1}{i/q} \cdot \frac{1}{\eta_T} \cdot \frac{1}{\tau_{res}} \qquad (3.8)$$

where the resolution time τ_{res} is the full width at half maximum of the coincidence peak.

From the viewpoint of statistical error analysis of the count rate and of experimental measuring time, a ratio $N_t/N_r \simeq 1$ is desirable. Thus it becomes obvious from equation (3.8), that for a given (or experimentally expected) probability P(b), one has to adjust the target gas density and the beam current accordingly. In addition it is advisable to chose a detection system with the appropriate efficiency and solid angle to keep the time needed to perform the experiment in an acceptable range.

Chapter 4

APPARATUS AND EXPERIMENTAL PROCEDURE

The experiment was performed at the James R. Macdonald Laboratory at Kansas State University using the model EN 6 MV Tandem Van De Graaff accelerator. A layout of the laboratory is shown in Figure 3. A Fluorine beam is accelerated to about 10 MeV and charge, mass and velocity analyzed in the primary 90^{o} analyzing magnet. The resulting 10 MeV F^{3+} beam of typically 4 to 6 μA was post stripped in a 10 $\mu g/cm^2$ carbon foil. Leaving the foil with a certain charge distribution, the beam is then analyzed in the second analyzing or switching magnet to a charge state of F^{6+}, F^{8+} or F^{9+} and directed into the beam line in use. On the way to the target gas region the beam passes through two magnetic quadupoles and is, over a length of 750 cm, tightly collimated by three adjustable slit systems (typically open to 3x3 mm, 1.5x1.5 mm and 1x1 mm), the last one serving as a beam scrapper to reduce slit scattering, and passed through an aperture of 2 mm diameter. After passing through the target gas region, the unscattered beam of about 1 to 1.5 mm diameter is collected on a small flag centered in the middle of the Parallel-Plate-Avalanche detector (PPAD) located 450 cm from the target region. The scattered projectiles are detected by the PPAD itself, covering a range of impact parameters from 0.05 to .46 a.u. Typical beam intensities for the various charge states on the different slit systems and on target are given in Table 1.

The electrons ejected from the target gas are analyzed by two electrostatic spherical sector analyzers with channel electron multipliers,

Figure 3. The Kansas State University J. R. Macdonald Tandem Van de Graaff Accelerator Laboratory.

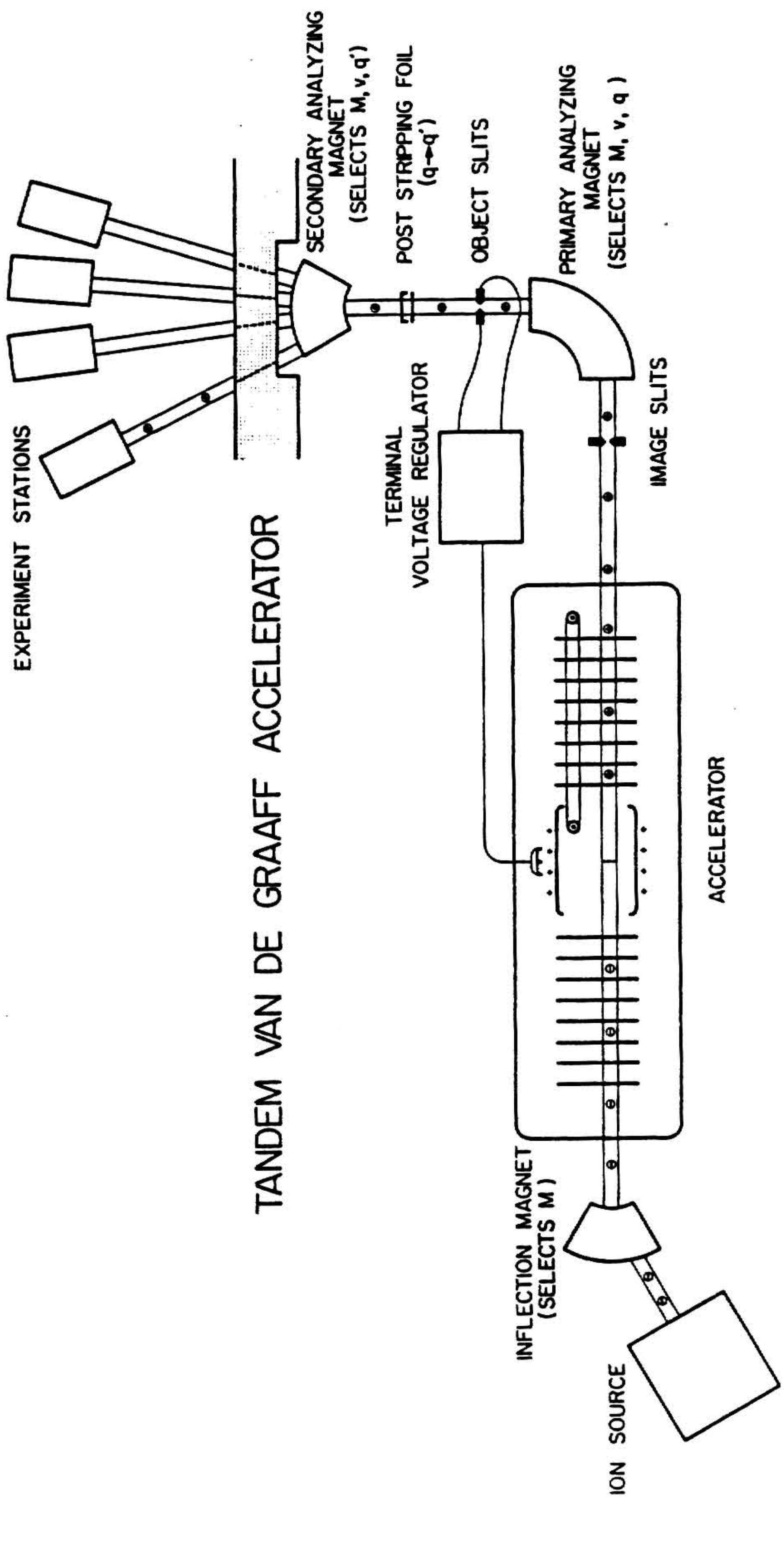
TANDEM VAN DE GRAAFF ACCELERATOR
EXPERIMENT STATIONS
SECONDARY ANALYZING MAGNET (SELECTS M, v, q')
POST STRIPPING FOIL (q→q')
OBJECT SLITS
PRIMARY ANALYZING MAGNET (SELECTS M, v, q)
TERMINAL VOLTAGE REGULATOR
IMAGE SLITS
ACCELERATOR
INFLECTION MAGNET (SELECTS M)
ION SOURCE

TABLE 1

Ion Beam Intensities

a) Primary Beam:

from ion source	∿15 μA	F^{1-}
from accelerator	∿20 μA	current beam
analyzed behind 90^{o} magnet	∿3-7 μA	F^{3+}

b) Poststripped Beams:

Beam Type	On Beam Scrapper	On Target
F^{6+}	∿50 nA	∿2-3 nA
F^{8+}	∿20 nA	∿5-1 nA
F^{9+}	∿.5 nA	∿15-30 pA

located opposite to each other on both sides of the beam. These spectrometers can be rotated independently to analyze electrons emitted at 52.5°, 90° and 127.5° with respect to the beam direction. The target gas is introduced into the target region via a gas needle producing a gas jet through and covering the whole beam cross section. A schematic diagram of the set-up is presented in Figure 4. In the following subsections the components of the experimental apparatus will be discussed in greater detail.

4-1) The Scattering Chamber

The scattering chamber is made out of a block of aluminum. It is manufactured as a double cross, each of the apertures having a diameter of 10.16 cm. One axis is aligned with the beam direction. From the top of the chamber the gas inlet in the form of a needle is mounted on a flange which can be moved horizontally in all directions. The needle can be lowered and optically aligned to be in a position just above the scattering center which is defined as the common focal point of the two electron spectrometers. The scattering chamber sits on top of a diffusion pump. This chamber-pump unit is supported by an adjustable stand and can be optically aligned to the beam axis. The two electron detection devices are fixed on both sides of the chamber.

At the beam entrance to the chamber a flange on which a small tubus with an end aperture of 2 mm diameter is centered, closes the chamber to the beam line. Only through this small opening as gas flow from the target region into the beam line is possible and thus ensures that the background pressure in the beam line could be kept well below $5 - 8 \times 10^{-7}$ Torr and only minimal pollution of the desired beam to lower charge states (mostly via electron capture) could occur. The beam exit from the chamber

Figure 4. Schematic of the beam collimating system and the experimental set-up.

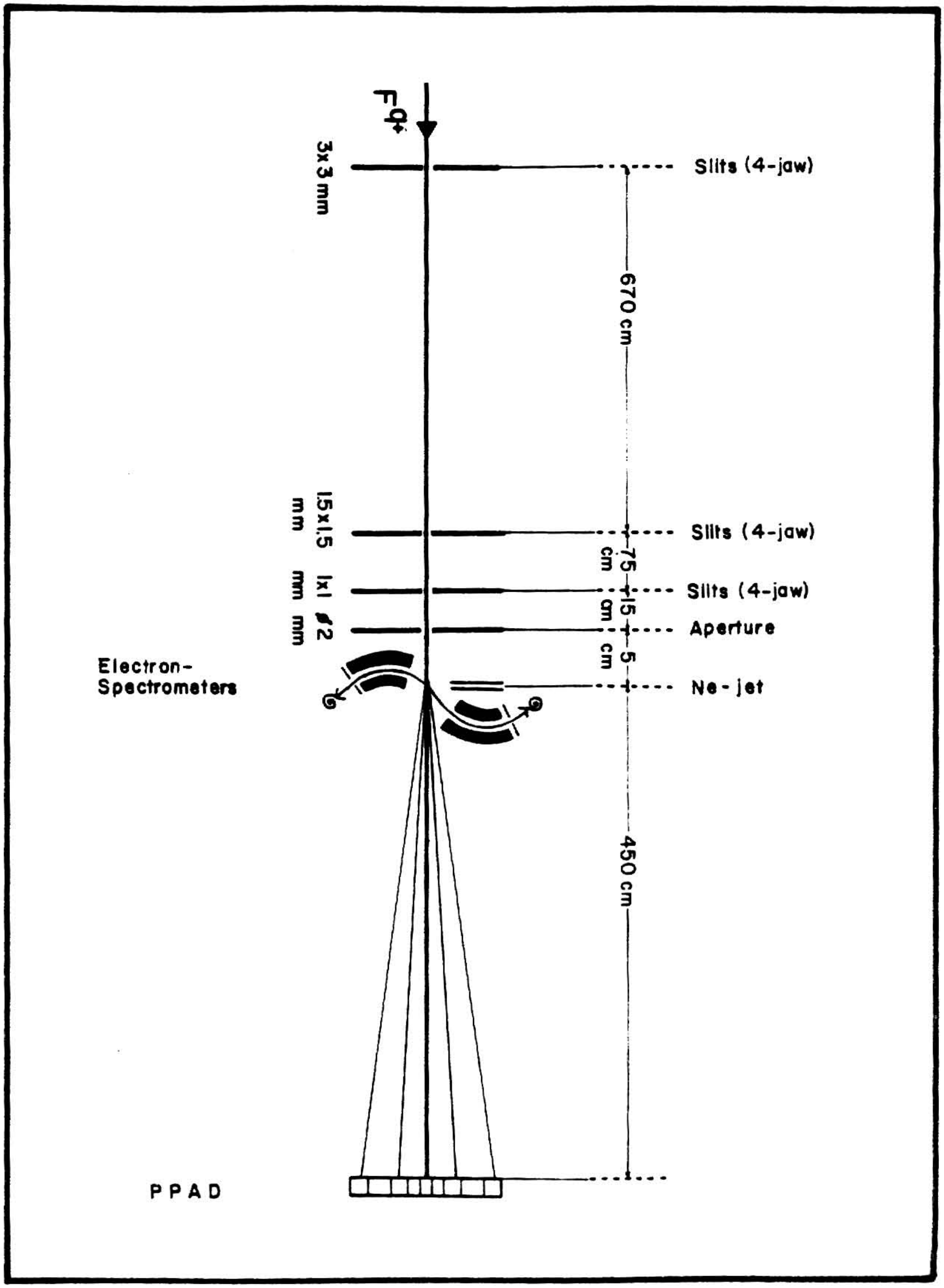

F^{q+}
3x3 mm
Slits (4-jaw)
670 cm
1.5x1.5 mm
Slits (4-jaw)
75 cm
1x1 mm
Slits (4-jaw)
15 cm
ø2 mm
Aperture
5 cm
Electron-
Spectrometers
Ne-jet
450 cm
PPAD

is, without further obstruction, directly connected to be the beam line. A diagram of the scattering chamber is shown in Figure 5.

4-2) The Electron Spectrometers

The two identical electron spectrometers have been built at Kansas State University. Each is housed in an aluminum cylinder which is lined by μ-metal to shield against external magnetic fields. The spectrometers can be moved on their support beams perpendicular to the ion beam axis without breaking the vacuum, thus ensuring that the focusing points coincide in one single point in the intersection of the ion beam and the gas jet and thus define a unique source volume for both analyzers.

The spectrometers themselves are electrostatic spherical sector analyzers (see Figure 6). The condensors consist of two spherical segments of $120^0 \times 88^0$ with an inner radius of $R_i = 32.5$ mm and an outer radius of $R_a = 37.5$ mm. They are made out of brass, are gold plated to supress contact potentials and are carbon coated to minimize the occurrence of secondary electrons. The entrances and exits of the condensors are closed by slits of 3mm width and 64^0 arc. These slits are designed to correct fringing fields according to Herzog specifications[37,38] and give an effective dimension of $120^0 \times 90^0$ to the spectrometers. From these dimensions the distance from the source volume to the entrance slits and from the exit slits to the electron detector amounts to 29.74 mm and the effective solid angle subtended by each spectrometer, given by[38]

$$d\Omega = \frac{100}{4\pi} \cdot \int_{-\beta/2}^{+\beta/2} \int_{\gamma-\alpha/2}^{\gamma+\alpha/2} \sin\gamma' \cdot d\gamma' \cdot d\beta' \quad \text{in \% of } 4\pi \qquad (4.1)$$

where $\gamma = 45^0$ is specified by the dimensions of the condensor including the effect of the slits, $\alpha = 5.8^0$ is determined by the width and $\beta = 21^0$ by the length of the entrance and exit slits, is thus calculated to be

Figure 5. Schematic of the scattering chamber.

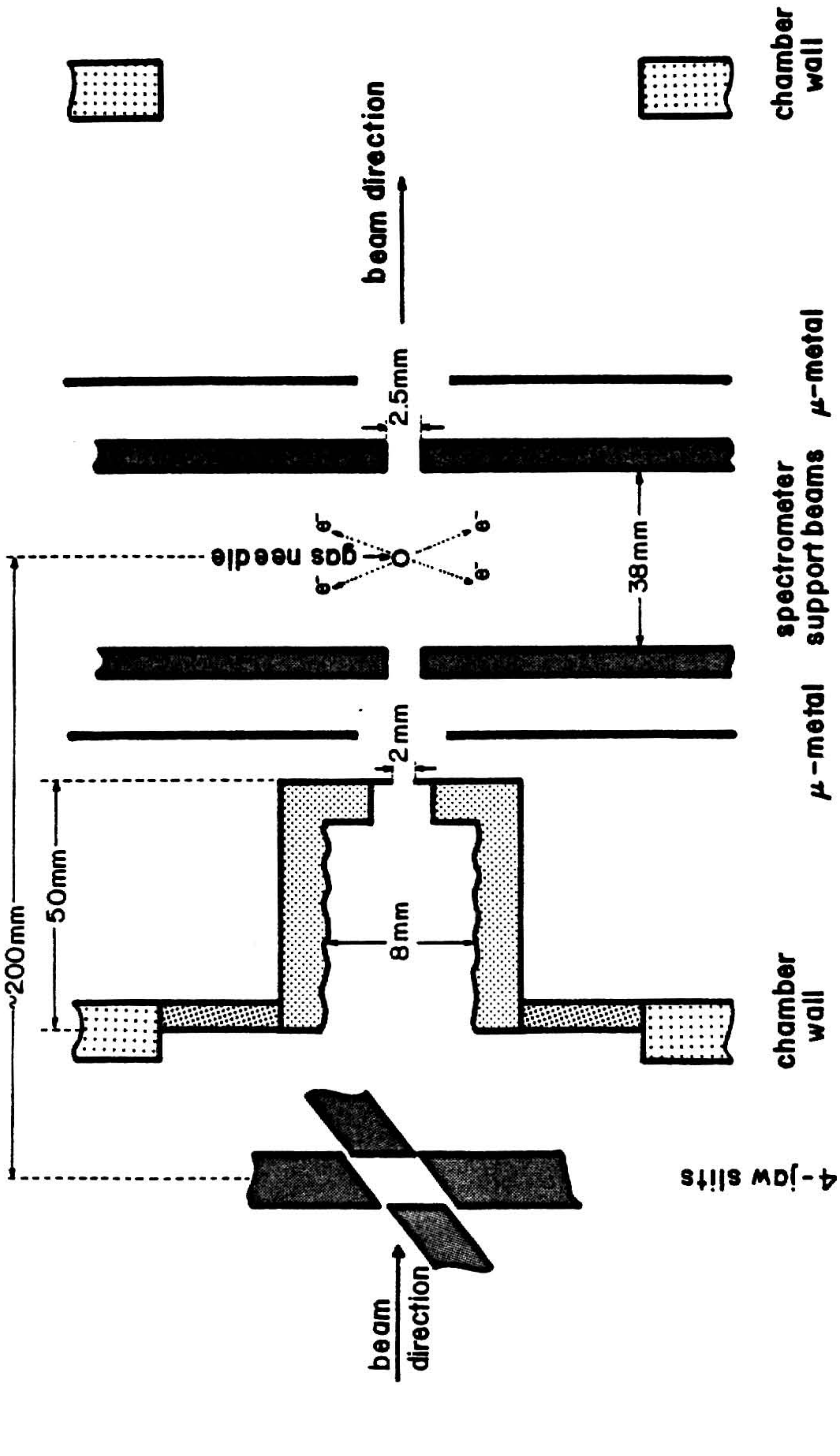
beam direction
chamber wall
μ-metal
2.5mm
spectrometer support beams
38mm
gas needle
e⁻
μ-metal
2mm
50mm
~200mm
8mm
chamber wall
4-jaw slits
beam direction

Figure 6. Schematic of the spherical sector electron analyzers.

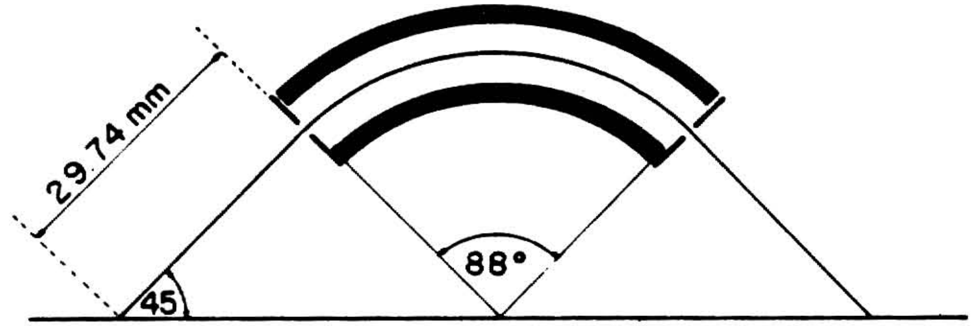

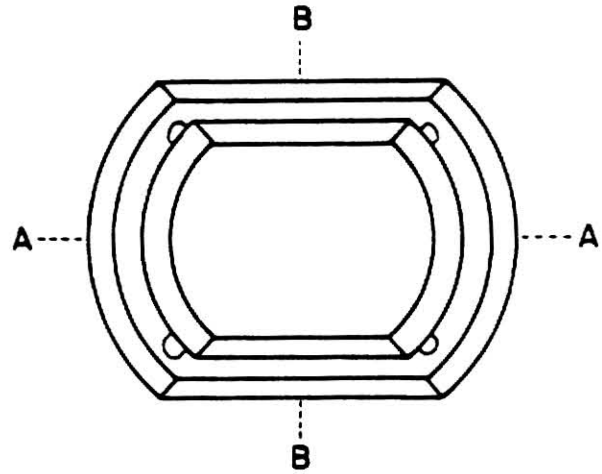

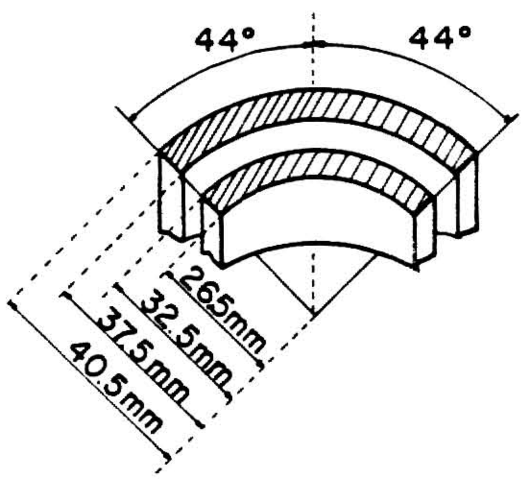

cut along B—B

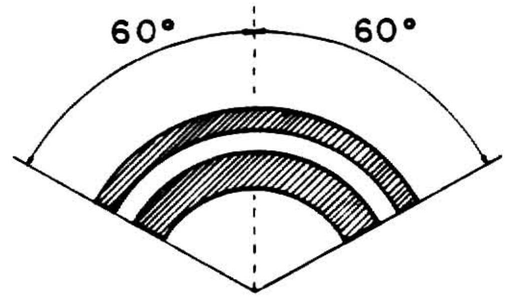

cut along A—A

5×10^{-2} sr. Two electron spectrometers were used mainly to double this solid angle and thus to reduce data taking time.

The electrons produced in the source volume enter the condensor through the entrance slit, pass through the condensor in which a selective potential field given by[39]

$$\Phi(r) = \Delta U \cdot \frac{R_i \cdot R_a}{R_a - R_i} \left\{ \frac{1}{r} - \frac{2}{R_a + R_i} \right\} \qquad (4.2)$$

where ΔU is the potential difference between the condensor plates, exists, leave the condensor through the exit slit and are detected by a channel electron multiplier (channeltron or CEM) housed in an aluminum cylinder. This cylinder is insulated from ground by teflon disks and at its entrance has a slit system which is set to give an energy resolution of about 2.5%. The CEM cone is kept on a negative potential of 100 to 200 V to supress background electrons, the anode is kept on +2400 V.

To energy analyze the electrons, the inner segment of the condensor is kept on a sweeping potential U_+ of 0 to +300 V, the outer segment on a simultaneously sweeping potential U_- of 0 to -300 V ($U_+ = |U_-| = U$). For a circular flight pass through the analyzer, the ratio of the accelerating voltage U_o ($U_o = E_e/e$) to the potential between the condensor segments ΔU ($\Delta U = U_+ - U_-$) is the spectrometer factor f, given by

$$f = \frac{U_o}{\Delta U} = \frac{U_o}{2U} \qquad (4.3)$$

f depends only on the geometry of the condensor itself and is for a spherical sector analyzer[38]

$$f = \frac{R_i \cdot R_a}{R_a^2 - R_i^2} \qquad (4.4)$$

With the given specifications of the spectrometer, f calculates to f=3.482.

It is most convenient to introduce a relative spectrometer factor f'[38] which is related to the equal, but in sign opposite potentials on the condensor segments. Then

$$f' = \frac{U_o}{U} = \frac{U_o}{U_+} = \left|\frac{U_o}{U_-}\right| = 2\ f = 6.964. \qquad (4.5)$$

f' gives a direct relation between the desired energy of the electrons to be analyzed and the voltage to be applied on the analyzer segments by

$$E_e = e \cdot U_e = f' \cdot e \cdot U \qquad (4.6)$$

Thus, for a sweeping voltage U from 0 to 300 V electrons with an energy ranging from E_{min} to 2100 eV will be recorded in the detector, where E_{min} is determined by the negative potential on the CEM cone.

The spectrometers can be rotated around their axis perpendicular to the beam axis and it is possible to detect electrons under a variety of emission angles, thus making a determination of angular dependence available. In the present experiment the analyzers are used in three different settings. If the condensor is adjusted symmetrically to an axis perpendicular to the beam (Figure 7a), electrons under an emission angle of $90^o \pm 21^o$ relative to the beam axis are observed. Is the analyzer rotated 1/4 turn into the beam direction (Figure 7b), an emission angle of $52.5^o \pm 7.5^o$ is covered, and in the case that the analyzer is turned 1/4 turn against the direction of the beam (Figure 7c), electrons emitted under $127.5^o \pm 7.5^o$ with respect to the beam are analyzed. The range of the different angles depends directly on the finite dimensions of the entrance and exit slits of the spectrometer.

4-3) The Parallel-Plate-Avalanche Detector (PPAD)

This detector - along with its supplementing electronics - was made available by H. Schmidt-Boecking and R. Schuch and was constructed at the

Figure 7. Positions of the electron analyzers relative to the beam direction.

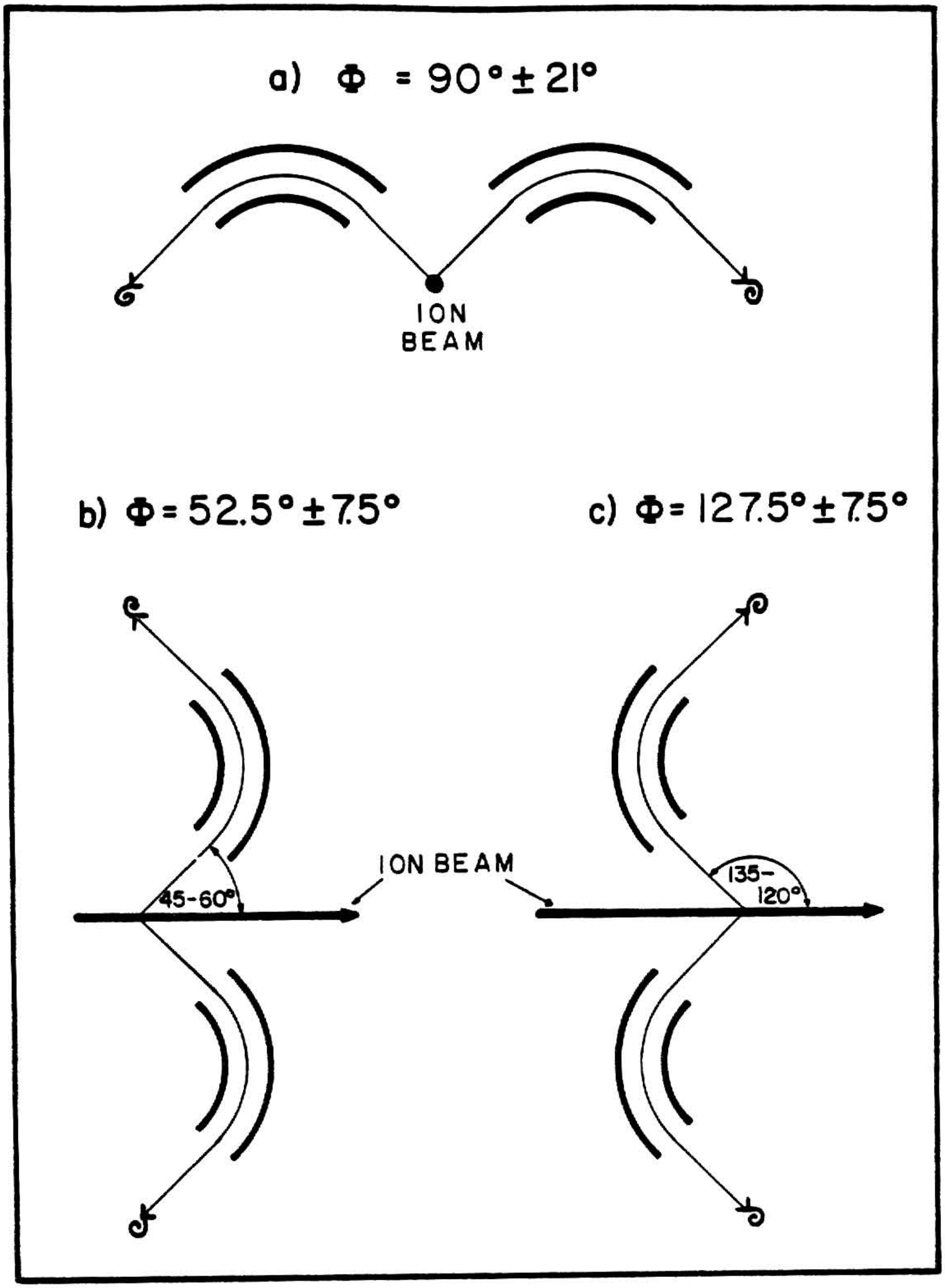
a) Φ = 90° ± 21°
ION
BEAM
b) Φ = 52.5° ± 7.5°
c) Φ = 127.5° ± 7.5°
ION BEAM
45-60°
135-
120°

Universitaet Heidelberg, W. Germany. It grew out of the interest for impact parameter measurements of heavy ions, which up to the first construction of this kind of PPAD[40] were limited by the use of mostly surface barrier detectors,[41-44] because these are restricted by high counting rates and are rapidly damaged by heavy ion impact.

The detector in use during this experiment is a 16 - annulus PPAD that makes the detection of particles scattered into different scattering angles during one experimental run possible. An outline of the detector is given in Figure 8.

The PPAD consists of two parallel electrodes, the potential grid and the 16 collector rings. They are separated by a gap filled with a gaseous atmosphere. To maintain this high pressure compared to the vacuum of 5×10^{-7} Torr in the beamline, a thin aluminized plastic foil, supported by a grid, closes the detector on the particle entrance side. The supporting grid features a beam stopper of about 3 mm diameter in its center. Part of this beam stopper is insulated and is used as a flag to monitor the direct beam of projectiles. The gaseous atomsphere within the detector is maintained by a constant flow of isobutane resulting in an effective pressure of about 20 to 25 Torr.

The scattered heavy ions are allowed to pass the supporting grid, the foil and the potential grid (all on ground potential). A positive high voltage of typically 600 V is applied through load resistors (100 kΩ) to the collecting rings. The strong field across the electrodes accelerates the free electrons and ions produced by the heavy ion impact in the isobutane, thus causing Townsend avalanches[45] and a resulting fast potential change on a collector ring. This signal is fed via a coupling capacitor (4.7 nF) into a fast preamplifier. Since each collector ring is connected

Figure 8. Schematic of the Parallel-Plate-Avalanche Particle Detector (PPAD).

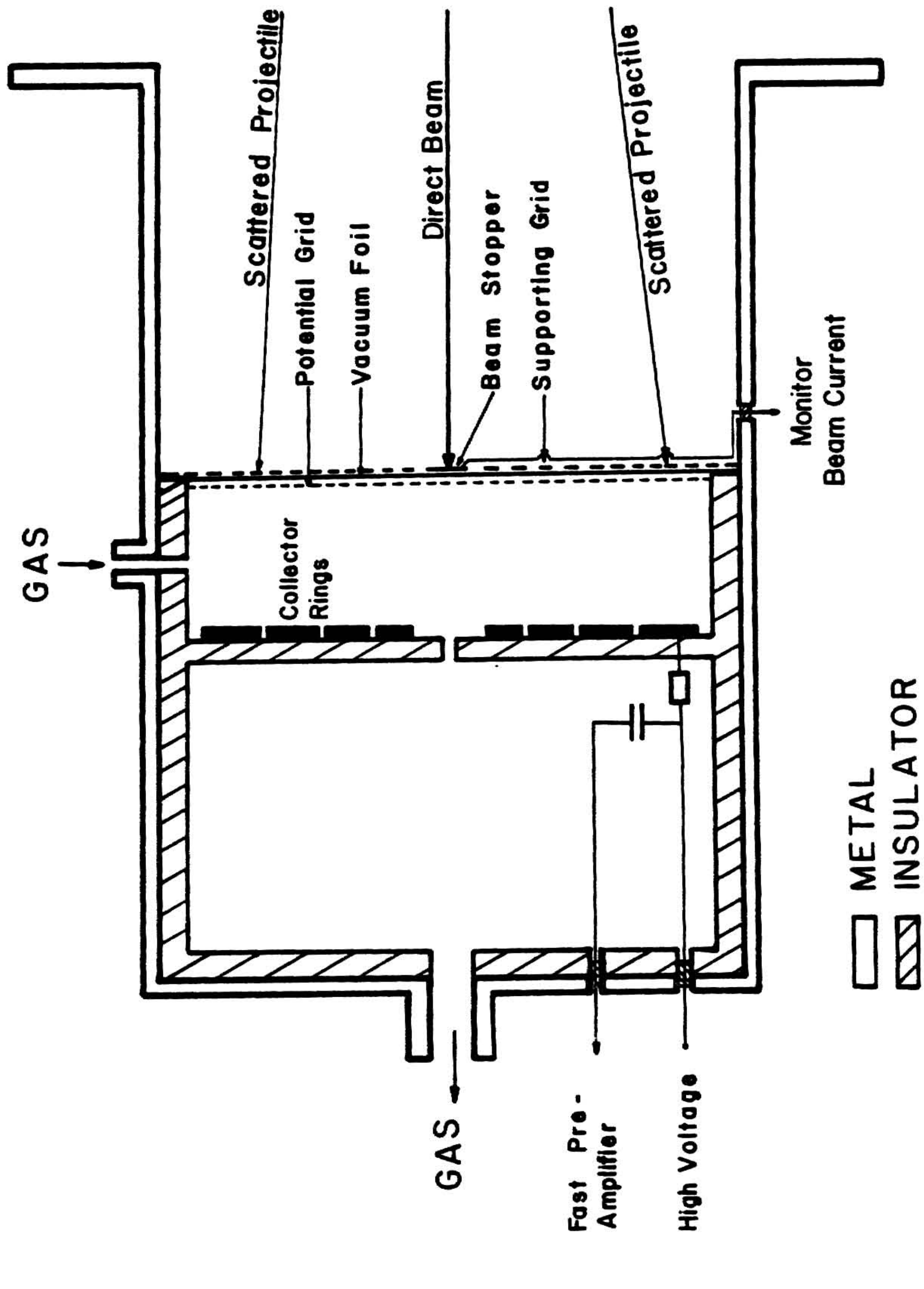
Scattered Projectile
Potential Grid
Vacuum Foil
Direct Beam
Beam Stopper
Supporting Grid
Scattered Projectile
Monitor
Beam Current
GAS
Collector
Rings
GAS
Fast Pre-
Amplifier
High Voltage
METAL
INSULATOR

to its own preamplifier, a simultaneous measurement of particles scattered into different scattering angles is possible.

The diameters of the rings range from 3.3 mm to 42.9 mm and their width is chosen to give a ±5% uncertainty to the impact parameters.

4-4) The Electronics Set-Up

The method used to register the signals from the electron analyzer CEM's and the PPAD is a standard, somewhat extended fast-slow-coincidence technique. An overview of the set-up is shown in Figure 9.

The total electronics array can be grouped into three parts.

a) Electron Detection Branch

Signals from the CEM's are fed into two preamplifiers, whose fast positive output signals are given in one case into a timing filter amplifier (TFA) followed by a constant fraction discriminator (CFD), in the other case into an arc timing amplifier (AT) combining the functions of a TFA and CFD in one unit. The resulting slow positive pulses are fed into the gate inputs of two linear gates (LG) which are driven by a positive signal from the spectrometer power supply proportional to the sweep voltage, but reduced in amplitude by a divider. The positive slow signals from the LG's are combined in a multiplexer and from there routed to an analog-digital-converter (ADC).

b) Particle Detection Branch

Signals from the 16 collector rings in the PPAD are fed independently into a 16-channel fast preamplifier and from there into two 16-channel "Kammerausleselogiken". These units assign to each channel a signal of definite pulse height between 0.5 and 8 V. Due to the high counting rates which could not be handled by the data processing and storage devices available in the laboratory, one "Kammerausleselogik" is gated by negative

Figure 9. Schematic of the electronics set-up supporting the electron and scattered particles detection systems.

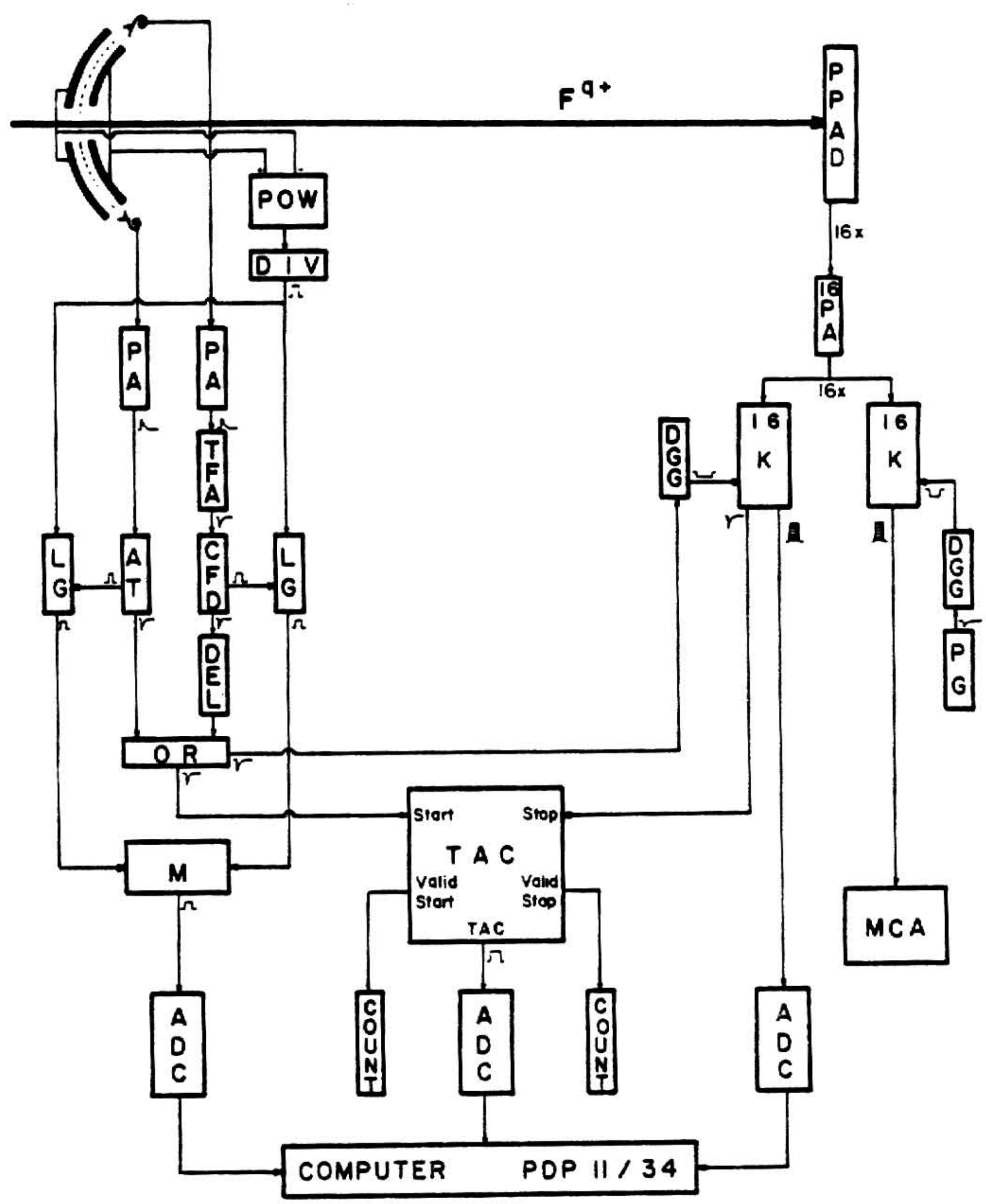

POW	Power Supply	16 PA	16-Channel Preamplifier
DIV	Devider	16 K	16-Channel Kommerauslesslogik
PA	Preamplifier	DGG	Delay and Gate Generator
TFA	Timing Filter Amplifier	PG	Pulse Generator
CFD	Constant Fraction Discriminator	MCA	Multichannel Analyzer
AT	Arc Timing Amplifier	TAC	Time Amplitude Converter
LG	Linear Gate	ADC	Analog Digital Converter
DEL	Nanosec. - Delay	COUNT	Counter
OR	Fast-Slow-Coincidence in "OR" mode	M	Multiplexer

fast random pulses from a pulse generator which are modified in a dual gate generator to a width of about 500 nsec and a repetition time of typically 300 to 500 μsec. The resulting scaling factor is determined. The positive gated signals from the "Kammerausleselogik" are given to a multichannel analyzer (MCA) resulting in a spectrum of 16 peaks.

c) TAC Branch

This part combines the signals from the electron detection and the scattered particle detection branch to yield a time delay spectrum of random and real coincidences (see also Chapter 3).

The fast negative signals from the CFD are put through a delay of typically 60 nsec and combined with the fast negative signals from the AT in a fast-slow-coincidence unit (OR) in "OR" mode. The fast negative signal resulting from the OR from both electron detection systems is fed as "start"-signal into a time-amplitude-converter (TAC). A second fast negative signal from the OR is delayed by 250 nsec and modified to a width of about 300 nsec in a delay-and-gate generator to compensate for the time of flight of the scattered projectiles from the target region to the PPAD and is used to gate the second 16-channel "Kammerausleselogik", which is necessary due to high counting rates and to limit the number of "stop"-signals in the TAC to those originating in true or random coincidence events. The slow positive signal from this unit is fed into an ADC, the fast negative signal is used as a "stop"-signal at the TAC. A window of accepted time delays in the TAC was set to 1 μsec. Time delays between start and stop signals within this range are given as a positive signal into an ADC, resulting in the TAC spectrum.

The three ADC's are connected to the computer system PDP 11/34. Spectra are recorded in a three-parameter list mode and stored on magnetic tape and floppy disks for later data analysis and evaluation.

4-5) Experimental Procedure

A beam of the desired charge state is brought into the target region with the slit systems set to about double their opening used during data taking runs. The resulting higher beam intensity allows for easier focusing and checking of the electron spectra. Fine focusing is done with two magnetic quadrupoles 150 cm in front of the first slit system. For each beam time period these quadrupoles have to be aligned vertically and horizontally with the actual beam axis to assure their focusing properties without steering the ion beam. In a later stage of the experiment a small deflecting magnet was installed between the quadrupoles and the first slit system to compensate this steering. The beam diameter and position can optically be checked by two viewers (fluorescent screens which could be moved into the ion beam), located between first and second set of slits and 25 cm in front of the scattering chamber. At this time the gas needle can be fine adjusted to avoid any scattering of projectiles off the needle, at the same time keeping the needle as close as possible above the focusing points of the electron spectrometers. The beam is then collimated down to a size of 1 to 1.5 mm diameter. A plexiglas blank-off flange with the exact dimensions of the PPAD baseplate is used at the position of the PPAD to visually inspect the size of the beam on a fluorescent screen. By centering the plexiglas flange it is assured that the beam spot coincides with the flag in the center of the later to be installed PPAD. The plexiglas flange is then removed and the PPAD put in place. After establishing the isobutane flow and positive high potential on the collector rings, Neon gas is let through the needle into the target gas region and the timing of the electronic units is adjusted. The discriminator level for each of the 16 channels of the Kammerauslesezlogik is fine tuned to eliminate cross talk between different channels. By inspecting the count rate of the PPAD in each channel with and without Neon in the target region, the slitscattering contribution to the count rate is determined and minimized by adjusting the beam scrapper in front of the scattering chamber For the inner ten collector rings these contributions are typically 10 to 15%, for the outer rings they range from 30 to 50%. This procedure is repeated after each run. In the case that the beam has to be brought into the target region on a different trajectory (due to the ion source switching its running mode) or after the change of focusing or other beam properties, the PPAD has to be adjusted to the new trajectory following the complete procedure described above.

The Neon gas pressure in the target gas region can not be determined directly. It is monitored by a thermocouple gauge in the foreline of the diffusion pump under the scattering chamber. From relative total electron production cross sections, Hagmann et al.[34] estimated a pressure of 150 to 200 mTorr in the target region over a beam length of 3 to 4 mm. After all adjustments are made, repeated data taking runs of typically ten hours duration are started. Between each two runs, the slitscattering contribution is determined.

For the data presented in this work, total beam-on-target time for data taking (not including time necessary for set-up, adjustments and slitscattering control) amounted to:

for 10 MeV F^{9+}, $\phi = 90.0^o$:	95 hours
for 10 MeV F^{9+}, $\phi = 52.5^o$:	38 hours
for 10 MeV F^{9+}, $\phi = 127.5^o$:	90 hours
for 10 MeV F^{8+}, $\phi = 90.0^o$:	27 hours
for 10 MeV F^{6+}, $\phi = 90.0^o$:	26 hours

Chapter 5

EXPERIMENTAL RESULTS AND THEIR COMPARISON TO A THEORETICAL MODEL CALCULATION

Before the delta-electron emission probabilities in 10 MeV F^{q+} + Ne could be investigated, several tests of the set-up have been undertaken. These tests are done without applying any coincidence conditions on the collision systems and involved several types of projectiles and targets, namely .5 MeV/u C^{6+}, N^{6+}, F^{6+} and F^{8+} on Helium and 1 MeV/u H^{1+}, F^{6+}, F^{8+} and F^{9+} on Neon. The evaluation of these data and the results are given in Section 5-1. The delta-electron emission probabilities as a function of the impact parameter, the delta-electron energy and the delta-electron emission angle have been measured for the systems 10 MeV F^{q+} + Ne, q=6, 8, 9. Their data evaluation and results are presented in Section 5-2. Section 5-3 will contain a discussion of the errors to which the obtained data are subject to. The principles of the Semiclassical Approximation and the corrections undertaken to extend this model into the region of this experiment are outlined in Section 5-4 and a comparison of an actual calculation with the results of this experiment will be given.

5-1) Double Differential Cross Sections (DDCS)

The collision systems .5 MeV/u C^{6+}, N^{6+}, F^{6+} and F^{8+} on Helium and 1 MeV/u H^{1+}, F^{6+}, F^{8+} and F^{9+} on Neon have been investigated to test the electron spectrometers and to gain knowledge about the energy distribution of the delta-electrons. The electrons were detected at $\phi = 90^{o}$ and in the case of F^{9+} impinging on Neon also at $\phi = 52.5^{o}$. Typical electron spectra are shown in Figure 10a-c.

Figure 10. Typical electron spectra recorded in

a) 10 MeV F^{6+} + Ne, $\phi = 90.0^{o}$

b) 10 MeV F^{9+} + Ne, $\phi = 90.0^{o}$

c) 10 MeV F^{9+} + Ne, $\phi = 52.5^{o}$

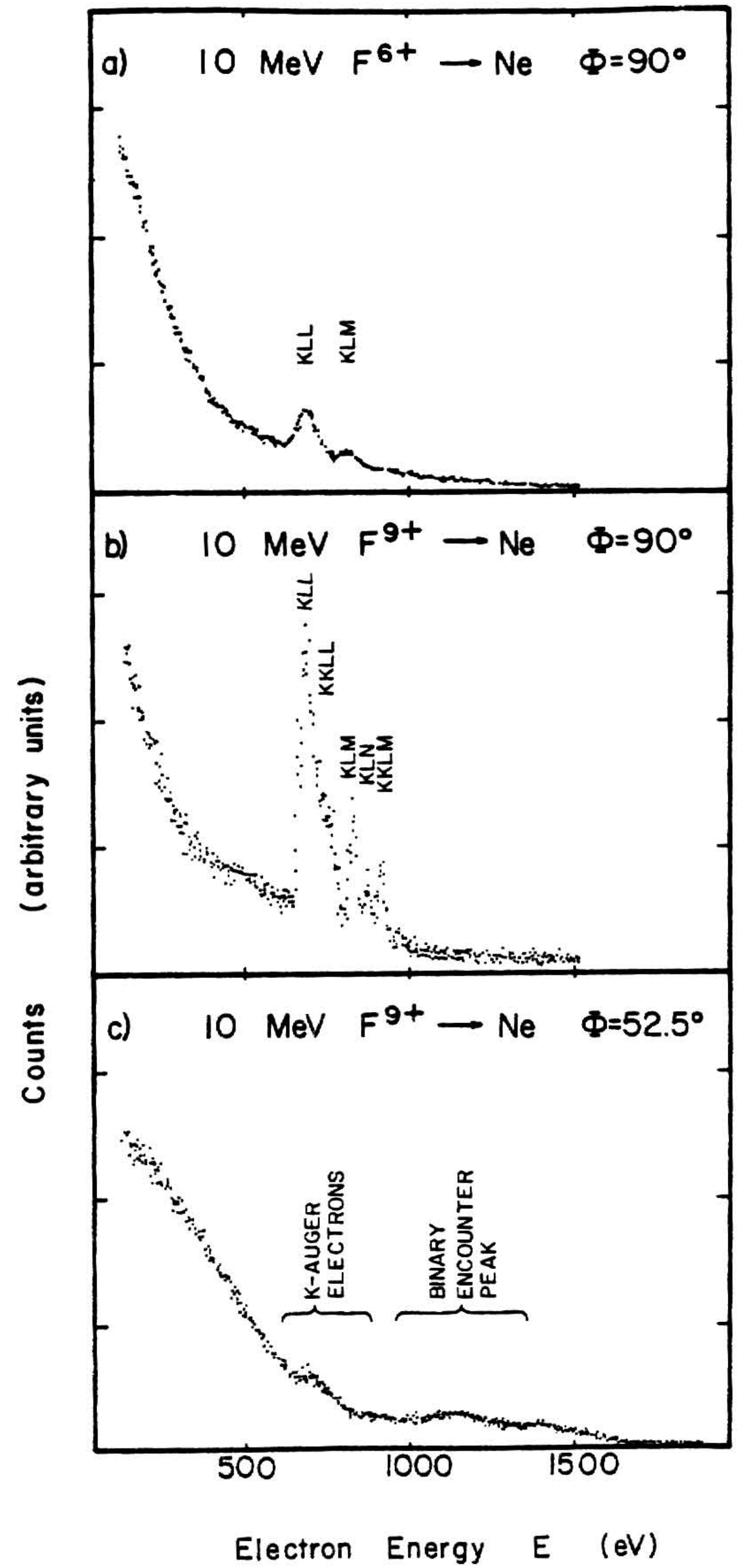
a) 10 MeV F^{6+} → Ne Φ=90°
KLL
KLM
b) 10 MeV F^{9+} → Ne Φ=90°
KLL
KKLL
KLM
KLN
KKLM
c) 10 MeV F^{9+} → Ne Φ=52.5°
K-AUGER ELECTRONS
BINARY ENCOUNTER PEAK
Counts (arbitrary units)
500
1000
1500
Electron Energy E (eV)

5-1, i) Data Evaluation

Since the position and energy of Neon K-Auger satellite and hypersatellite lines following F^{q+} impact are known experimentally,[34,46-48] all obtained electron spectra can be energy calibrated to within an uncertainty of ±2 eV. During data taking runs the beam current is integrated and recorded. The electron count rate due to background (without target gas) is determined and delta-electron spectra can thus be background-corrected. Since the gas target density cannot be determined precisely, only relative double differential cross sections DDCS in emission angle and electron energy can be obtained by normalizing the electron count rate to the integrated beam current and relative target gas density. The thus obtained results for the collision systems .5 MeV/u C^{6+}, N^{6+}, F^{6+} and F^{8+} on Helium are shown in Figure 11.

For the collision systems 1 MeV/u H^{1+}, F^{6+}, F^{8+} and F^{9+} on Neon, the absolute cross sections for the production of Neon K-Auger electrons is known.[48] Thus the count rate of delta-electrons can be normalized to these cross sections and absolute DDCS for these collision systems are obtained. The results are shown in Figure 12.

A comparison with data from Toburen et al.[7] show a constant efficiency of about 10% of the electron spectrometers in use over the range of observed electron energies.

5-1, ii) Results

In both Figures 11 and 12 it can be seen that the DDCS scale only approximately with Z_p^2, as predicted by PWBA, BEA and SCA models. In Figure 11 the cross sections scale (relative to the values obtained with C^{6+} as projectile, theoretical values in parenthesis)

Figure 11. Energy dependence of the relative double differential cross sections in .5 MeV/u Z^{q+} + He, $\phi = 90.0^{o}$

Z^{q+} = ·······△ C^{6+} —·—·■ N^{6+}

-------○ F^{6+} ——● F^{8+}

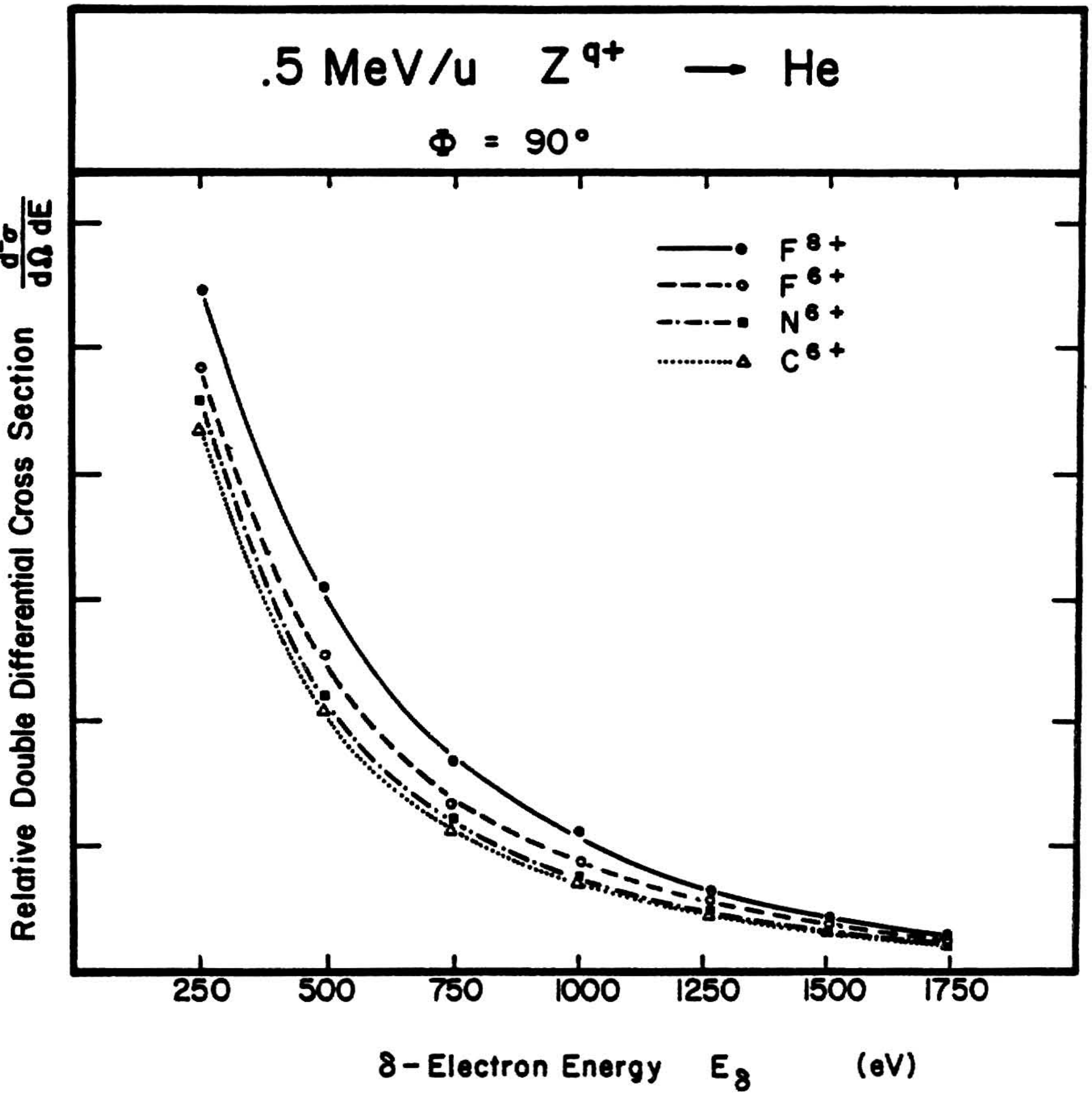
.5 MeV/u Z^{q+} → He
Φ = 90°
F^{8+}
F^{6+}
N^{6+}
C^{6+}
Relative Double Differential Cross Section $\frac{d^2\sigma}{d\Omega\, dE}$
250
500
750
1000
1250
1500
1750
δ - Electron Energy E_δ (eV)

Figure 12. Energy dependence of the absolute double differential cross sections in 1 MeV/u Z^{q+} + Ne, ϕ = 90.0^{o}

Z^{q+} = —·— ■ H^{1+} .... o F^{6+}

— — ▲ F^{8+} ——— ● F^{9+}

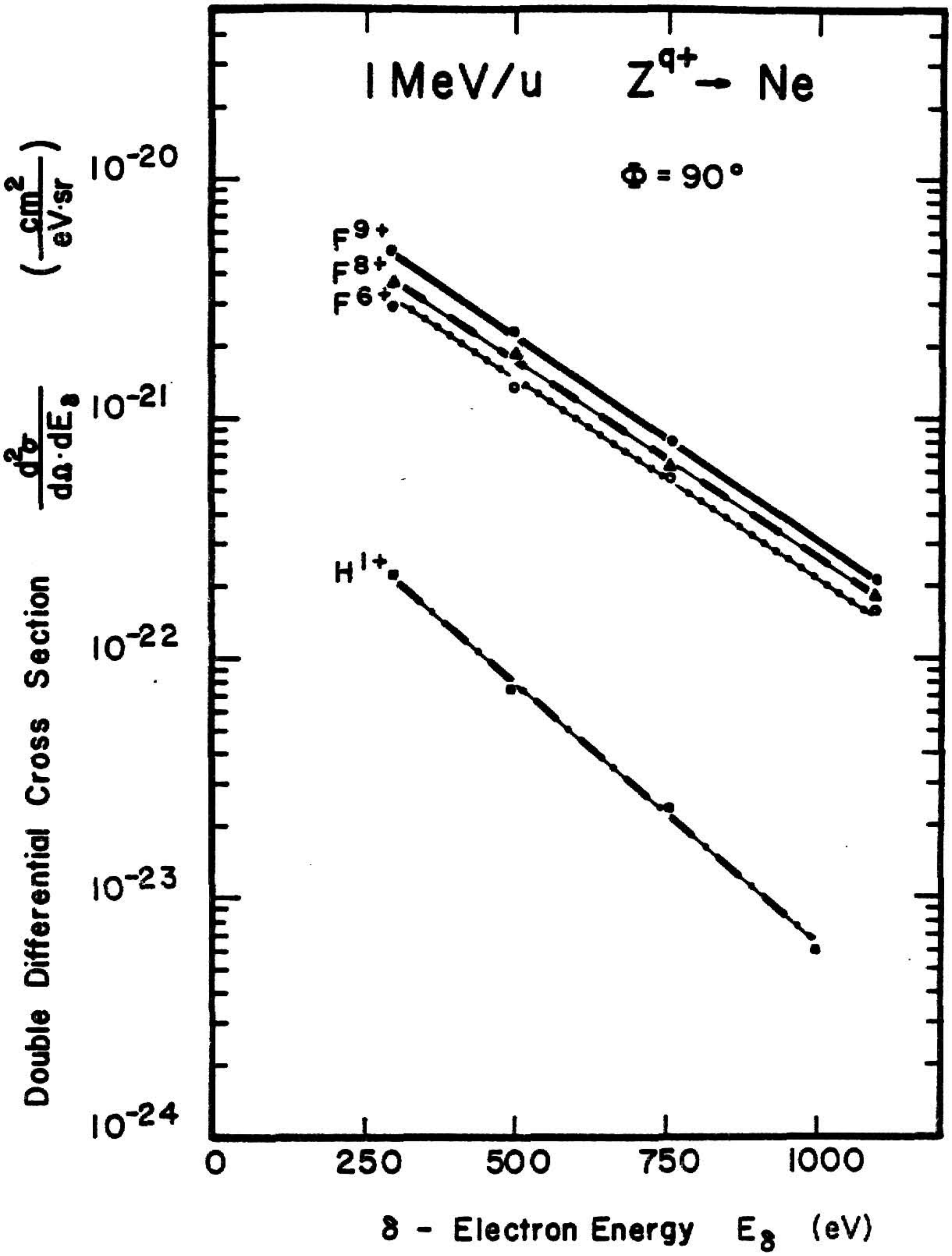
1 MeV/u $Z^{q+} \rightarrow$ Ne
$\Phi = 90°$
F^{9+}
F^{8+}
F^{6+}
H^{1+}
10^{-20}
10^{-21}
10^{-22}
10^{-23}
10^{-24}
0
250
500
750
1000
Double Differential Cross Section $\frac{d^2\sigma}{d\Omega \cdot dE_\delta}$ $\left(\frac{cm^2}{eV \cdot sr}\right)$
δ - Electron Energy E_δ (eV)

N^{6+}: 1.20 (1.35)

F^{6+}: 1.70

F^{8+}: 2.05 (2.25 for F^{q+})

and the cross sections for F^{6+} and F^{8+} scale only approximately with q^2, i.e. 1.50 (1.75).

For the second series of collision systems the absolute DDCS (Figure 12) scale with only about 75% of the theoretically predicted value Z_p^2=81 relative to the proton data.

It should also be noted that target electrons are the major contributors to the electron count rate observed at ϕ = 90^o and electrons brought into the collision by the projectiles play only a minor role. This is especially obvious in the second set of collision systems, since the cross sections obtained in collisions of lithium- and hydrogen-like Fluorine with Neon are about 20% and 10% lower than those obtained with bare Fluorine projectiles. From Figures 10a and b, 11 and 12 it can be seen that the delta-electron count rate and thus the DDCS observed at ϕ = 90^o fall off approximately in an exponential way with the electron energy. This shape has its origin in the momentum distribution of the target electrons.[49,50,52] This target momentum distribution is given as the absolute square of the wave function in momentum space $|\phi_j(p)|^2$, where

$$\phi_j(p) = (2\pi)^{-3/2} \int \psi_j(\vec{r}) \cdot e^{-i\vec{p}\cdot\vec{r}}\, d^3r \tag{5.1}$$

and is published by Weigold[49] for Helium and Neon.

If a projectile with momentum $\vec{p}_o$ collides with a target atom, the target nucleus will recoil with momentum $\vec{q}$ and an electron may be emitted with momentum $\vec{p}_e$, i.e. a momentum transfer $\vec{k}$ from the projectile to the target electron will take place, where

$$\vec{k} = \vec{p}_o - \vec{p}_o' \qquad (5.2)$$

with p_o' being the momentum of the projectile after the collision. If the target electron has a momentum $\vec{p}$ before the collision, it will have a momentum

$$\vec{p}_e = \vec{p} + \vec{k} \qquad (5.3)$$

after the collision. Here the assumption is made, that $\vec{p} = -\vec{q}$, i.e. one assumes a fast knock-out collision.

Since a wide range of momentum transfers is possible, the electron spectra will contain electrons with all possible momenta $\vec{p}_e = \vec{p} + \vec{k}$, but the shape of the momentum distribution will be approximately conserved.

Thus, for a Helium target the delta-electron energy dependence of the DDCS reproduces the shape of the momentum distribution of the 1s electrons, whereas the energy dependence of the DDCS for a Neon target represents the combined momentum distributions of the 1s, 2s and 2p electrons in Neon (where the contribution from the 1s electrons is small, as will be seen in Section 5-4.).

Rudd[53] tries to explain the exponential dependence of the electron count rate and the DDCS on electron energy by a promotion model of the target electrons into the continuum. As the projectile approaches the target, a charge transfer transition can take place. Then near the distance of closet approach a rotational coupling results in the promotion of the system to an excited state of either the projectile or the target. In either case, the state has an energy only a few eV below the ionization continuum. Finally, an energy transfer transition yields a free electron. Using the projectile velocity dependence of the rotational coupling given by Taulbjerg et al.[54] for near symmetric collisions and the probabilities for charge transfer given by Meyerhof,[55] Rudd finds an energy dependence of the electron emission cross sections as $\exp(-\alpha E_\delta \sqrt{186 \cdot Z_p / E_p \cdot E_B})$, where α is a dimensionless length parameter near unity. This picture incidentally gives the right energy dependence measured in this experiment (within 20%). However, the validity of its arguments for the collision systems considered here has to be questioned. In the case that the electrons are emitted at an angle $\phi < 90^o$ with respect to the beam direction (see Figure 10c for 10 MeV F^{9+} + Ne, $\phi = 52.5^o$), the energy dependence of the electron count rate has the same shape as for $\phi = 90^o$ for low electron energies. However, at higher electron energies an additional feature can be observed. Its origin is to be sought in the occurrence of a binary encounter peak of the Neon L-shell electrons. This peak can be explained in a classical picture. The cross section for the scattering of projectiles off free electrons as a function of the electron energy is a delta-function located at $E'(\phi)$, the energy the electron, moving into ϕ, picks up in the collision. Only the laws of conservation of energy and momentum are involved in calculating E'. Since the electrons bound in a Neon atom possess a binding energy E_B, the electrons forming the binary encounter peak have to overcome this binding energy to leave the atom and the binary encounter peak will be located at an energy $E = E' - E_B$, given by

$$E = \frac{4M_p m_o E_p}{(M_p+m_o)^2} \cos^2 \phi - E_B \qquad (5.4)$$

where M_p and E_p are the projectile mass and energy, m_o is the electron mass and ϕ is the angle at which the electrons are emitted. Since the bound target electrons have a momentum distribution and not a fixed value of momentum, this distribution has to be considered when applying the laws of conservation of momentum. Thus E' and E will be subject to this distribution and the binary encounter peak will be broadened out.

5-2) Delta-Electron Emission Probabilities

The following collision systems have been investigated to determine the delta-electron emission probabilities as a function of the impact parameter b, the delta-electron energy E_δ and the delta-electron emission angle ϕ:

10 MeV F^{6+} + Ne, $\phi = 90.0^o$

10 MeV F^{8+} + Ne, $\phi = 90.0^o$ and

10 MeV F^{9+} + Ne, $\phi = 52.5^o$, 90.0^o and 127.5^o

5-2, i) Data Evaluation

Raw data obtained during each run are stored in pulse-height analysis on floppy disks and in time-correlated list mode on magnetic tape. Typical electron spectra for F^{q+} on Neon ($q = 6, 9$; $\phi = 52.5^o, 90^o$) are shown in Figure 10a-c, a typical TAC spectrum is shown in Figure 13 and a coincident particle spectrum is shown in Figure 14.

The data stored on magnetic tape are sorted into a window set on the peak in the TAC spectrum, in which case one obtains a two dimensional spectrum of the coincident electrons originating from simultaneous interactions with projectiles scattered into all detected scattering angles. From these two dimensional spectra projections are made covering a single peak each in the coincident particle spectra. The thus obtained one dimensional spectra contain the electrons coincident with projectiles scattered into, and detected in, only one of the collector rings. Projections for all rings are made,thus yielding spectra of coincident electrons emitted in collisions involving different, fixed impact parameters (a schematic diagram of this process is given in Figure 15). The same procedure is repeated with the window in the TAC spectrum set to cover a region of random coincidences, thus yielding spectra of electrons

Figure 13. Typical time-delay (TAC) Spectrum recorded in 10 MeV F^{9+} + Ne, ϕ =52.5^{o}.

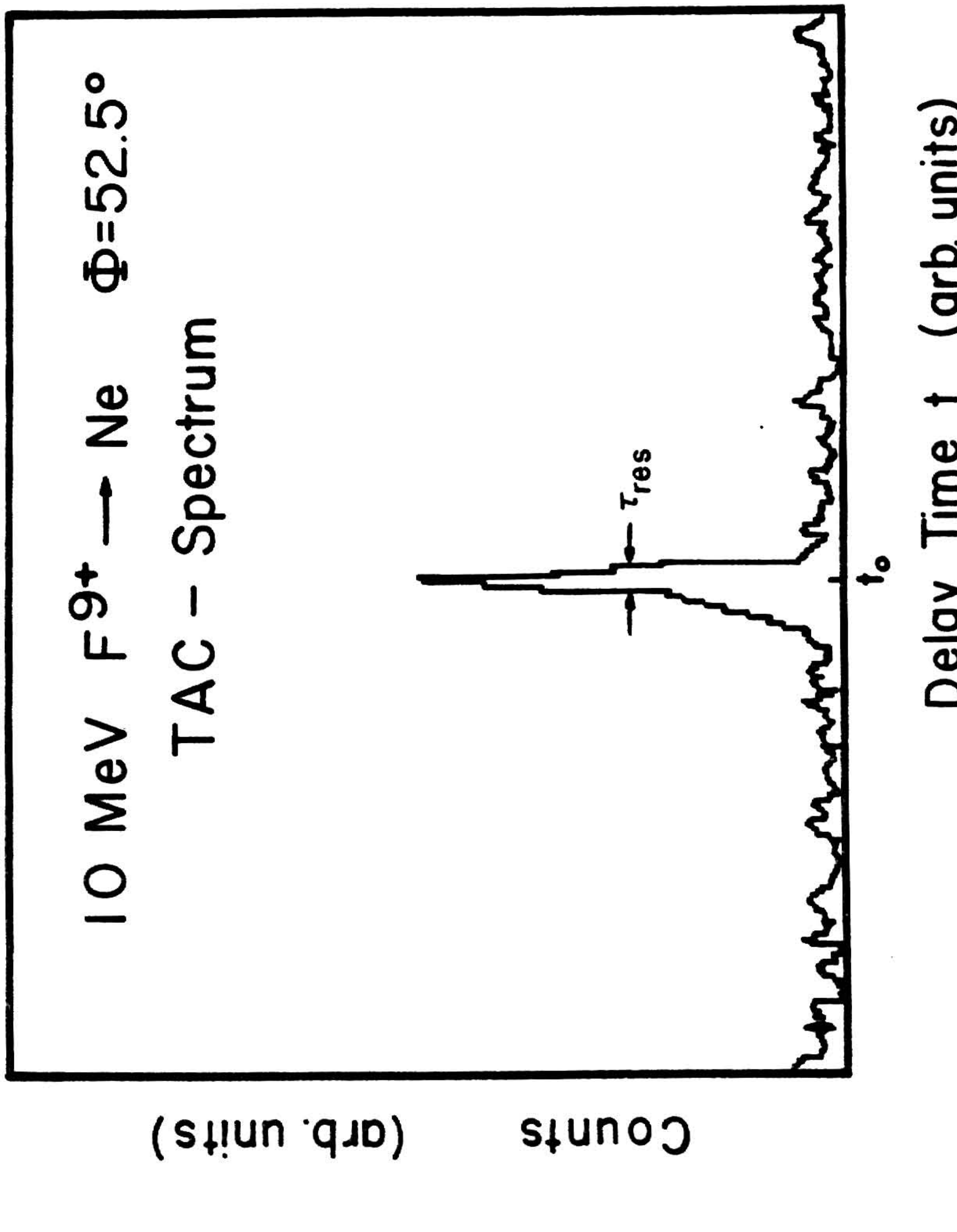
10 MeV F^{9+} → Ne $\Phi=52.5°$
TAC – Spectrum
τ_{res}
t_0
Delay Time t (arb. units)
Counts (arb. units)

Figure 14. Typical coincident particle spectrum recorded in 10 MeV F^{6+} + Ne, $\phi = 90.0^{o}$.

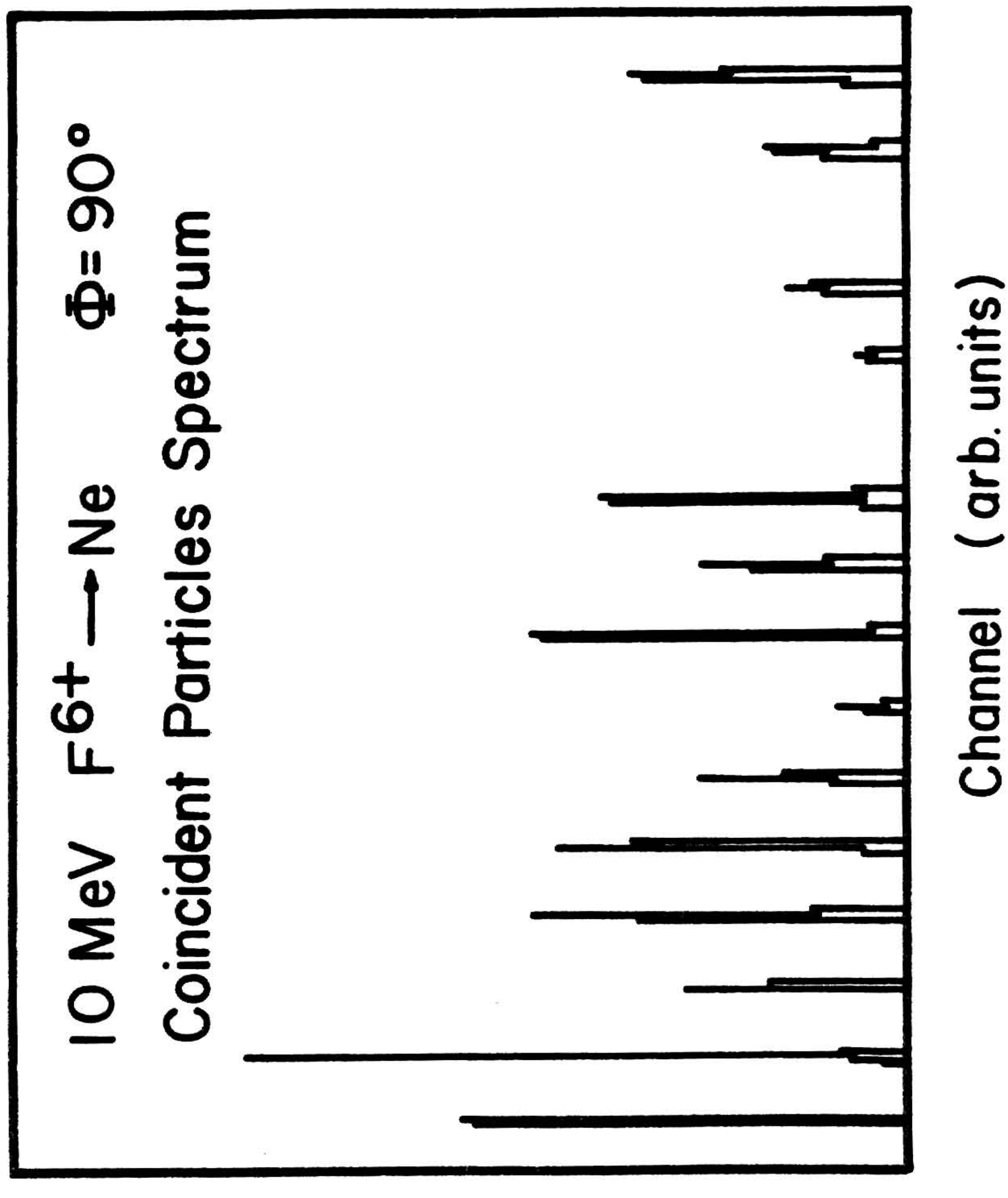

10 MeV $F^{6+} \longrightarrow Ne$ $\Phi = 90°$
Coincident Particles Spectrum
Channel (arb. units)
Counts (arb. units)

Figure 15. Schematic of the data evaluation process for coincidence measurements: sorting and projecting of spectra.

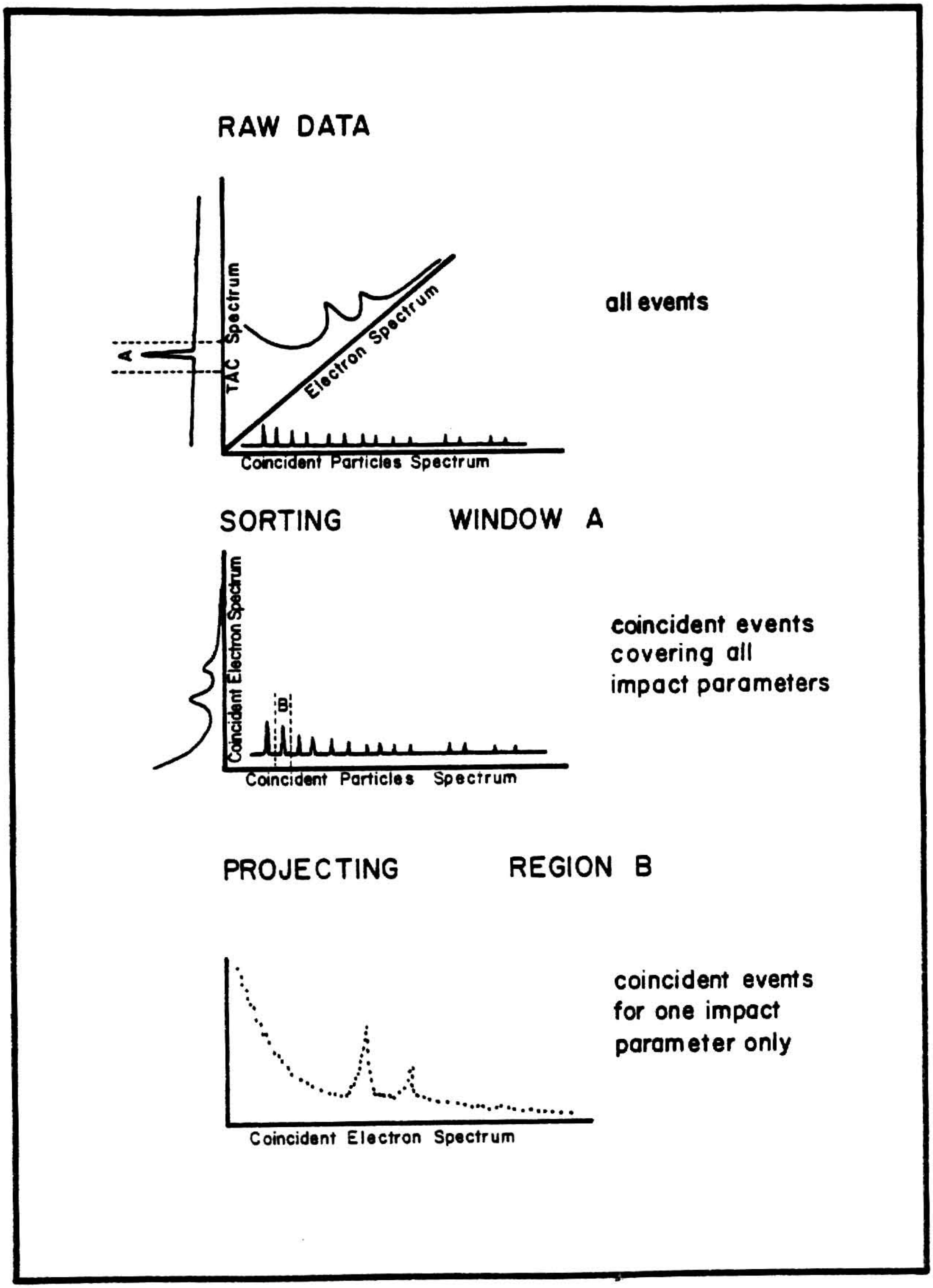
RAW DATA
TAC Spectrum
Electron Spectrum
A
Coincident Particles Spectrum
all events
SORTING
WINDOW A
Coincident Electron Spectrum
B
Coincident Particles Spectrum
coincident events
covering all
impact parameters
PROJECTING
REGION B
Coincident Electron Spectrum
coincident events
for one impact
parameter only

coincident with particles not originating in the same collision event. These random electron spectra have to be subtracted from the coincident electron spectra to obtain spectra of truly coincident electrons emitted in a collision event with a fixed impact parameter.

Since the position and the energy of the Neon K-Auger hypersatellite and satellite lines following F^{q+} impact are known,[34,46-48] the coincident electron spectra can be energy calibrated. Windows of 80 eV width are chosen around delta-electron energies E_δ = 275, 435, 535 and 1100 eV for all investigated collision systems and in the cases of 10 MeV $F^{6+,8+}$ + Ne, $\phi = 90^o$ and F^{9+}, $\phi = 52.5^o$ also around E_δ = 150, 975, 1300 and 1400 eV. The number of electrons in these windows is determined and is normalized to a width of 1 eV (yielding an uncertainty of ± 40 eV in delta-electron energy). Since the absolute probabilities as a function of impact parameter for the production of Ne-K-Auger satellite and hypersatellite electrons following F^{q+} impact are known (for F^{9+} + Ne see Ref. 46 and 47, for F^{6+} and F^{8+} + Ne see Ref. 34), the obtained raw data in the experiment presented here can be normalized to these known probabilities. Also necessary is a correction due to the finite size of the solid angle subtended by the electron analyzers and a correction in efficiency since the spherical sector analyzers in use feature a constant $\Delta E/E$. The probabilities for delta-electron emission in this experiment is given by equation (3.3)

$$P(b) = \frac{N_t}{N_p} \cdot \frac{1}{\varepsilon_e} \cdot \frac{1}{d\Omega_e}\ , \text{ which can thus be written as}$$

$$P(b,E_\delta,\phi) = \frac{N_\delta(b,E_\delta,\phi)}{N_K(b)} \cdot P_K(b) \cdot \frac{E_o}{E_\delta} \cdot \alpha \quad \left(\frac{1}{eV \cdot sr}\right) \tag{5.5}$$

where N_δ is the observed count rate of coincident delta-electrons in a window of 80 eV width around E_δ, originating in a collision with impact parameter b and emitted into an angle ϕ, N_K is the observed number of coincident Auger-electrons (for F^{9+} + Ne K-Auger hypersatellite electrons, for F^{6+} + Ne and F^{8+} + Ne K-Auger satellite electrons are used), P_K is the corresponding absolute probability for the production of these Auger-electrons,[34,46,47] E_0 is the energy to which these Auger-electrons are normalized to compensate for a constant $\Delta E/E$ and $\alpha = \frac{d\Omega_e}{80} = 5 \times 10^{-2}/80 = 6.25 \times 10^{-4}$ is a constant taking the finite size of the solid angle of the spectrometers and the width of the electron window into account.

To obtain N_K from the sorted and projected coincident electron spectra, several methods have to be applied.

As can be seen in Figure 10b, the number of delta-electrons underlying the peaks of K-Auger-electrons for F^{9+} + Ne in the case of $\phi = 90^o$ and 127.5^o is small compared to the number of K-Auger-electrons and negligible in the coincident electron spectra. Thus N_K can be obtained directly from these spectra. In the case of F^{8+} + Ne the delta-electrons amount to less than 10% under the Auger peaks, for F^{6+} + Ne they contribute up to 20%. In the coincident spectra these contributions are somewhat less and within the statistical error of the count rates. Thus no elaborate procedure is necessary to correct for these effects. However, in the case that the electron spectra are taken under forward angle (i.e. in this work F^{9+} + Ne, $\phi = 52.5^o$) one can observe (Figure 10c) a distinct contribution of delta-electrons underlying the Auger-peaks, and the additional binary encounter peak at higher energies. To compensate for all the electrons underlying the K-Auger electron peaks, a fit program written by M. Stoeckli[51] was used to obtain N_K.

To obtain P_K, a smooth curve was drawn through the experimental values published by S. Hagmann et al.[34,46,47] and the values corresponding to this curve are incorporated into equation (5.5).

As a control measure, the obtained P_K are divided by N_p, where N_p

is the number of off the target gas scattered projectiles with impact parameter b, i.e. the slitscattering contribution to N_p has been subtracted. The thus obtained relative probabilities for K-Auger electron emission reproduce the shape of the data measured by S. Hagmann et al. within statistical error.

By applying equations (3.3) and (5.5) to the raw experimental data, one obtains delta-electron emission probabilities $P(b,E_\delta,\phi)$ as a function of impact parameter b, delta-electron energy E_δ and emission angle ϕ, i.e. triple differential probabilities.

These triple differential probabilities can be presented in three ways:

a) as a function of the impact parameter b indicating the internuclear distance at which the emission of delta-electrons is most likely

b) as a function of the delta-electron energy E_δ, yielding the energy distribution of delta-electrons, and

c) as a function of the emission angle ϕ, thus providing information about the angular dependence of delta-electron emission.

5-2, ii) Results

a) Delta-Electron Emission Probabilities as a Function of the Impact Parameter b

The impact parameter dependence of the delta-electron emission probability for the various collision systems is presented in Figures 16 to 20.

Several features are observed:

Independent of the delta-electron energy E_δ, the charge state of the incoming projectile and the delta-electron emission angle ϕ, the delta-electron emission probability rises with increasing impact parameter to a maximum value and then falls off somewhat exponentially. The maximum

Figure 16. Impact parameter dependence of the delta-electron emission probability in 10 MeV F^{6+} + Ne, $\phi = 90.0^{\circ}$. The impact parameter is subject to an uncertainty of ±5%.

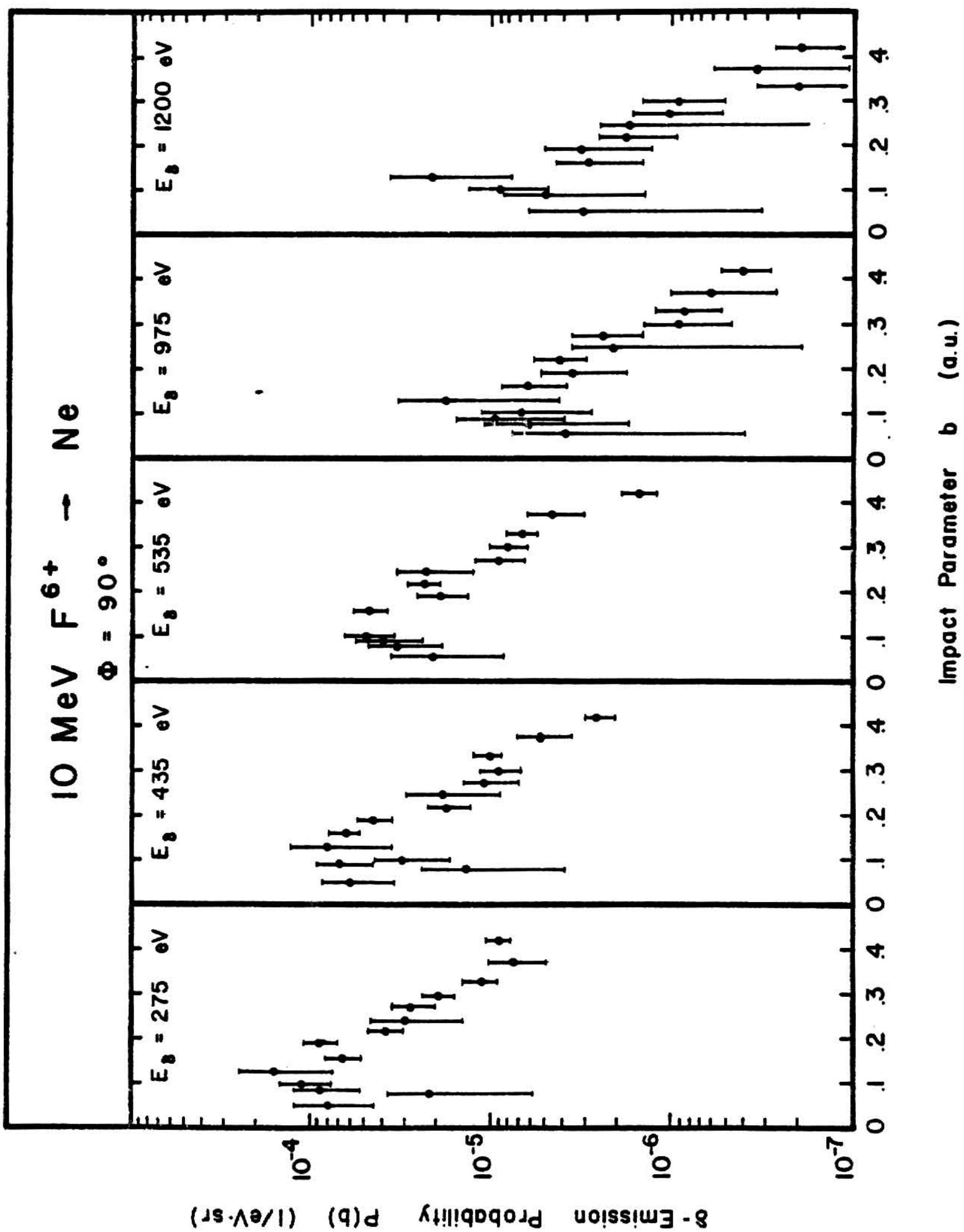

10 MeV F^{6+} → Ne
Φ = 90°
E$_δ$ = 275 eV
E$_δ$ = 435 eV
E$_δ$ = 535 eV
E$_δ$ = 975 eV
E$_δ$ = 1200 eV
Impact Parameter b (a.u.)
δ - Emission Probability P(b) (1/eV·sr)
10^{-4}
10^{-5}
10^{-6}
10^{-7}

Figure 17. Impact parameter dependence of the delta-electron emission probability in 10 MeV F^{8+} + Ne, $\phi = 90.0^{o}$. The impact parameter is subject to an uncertainty of ±5%.

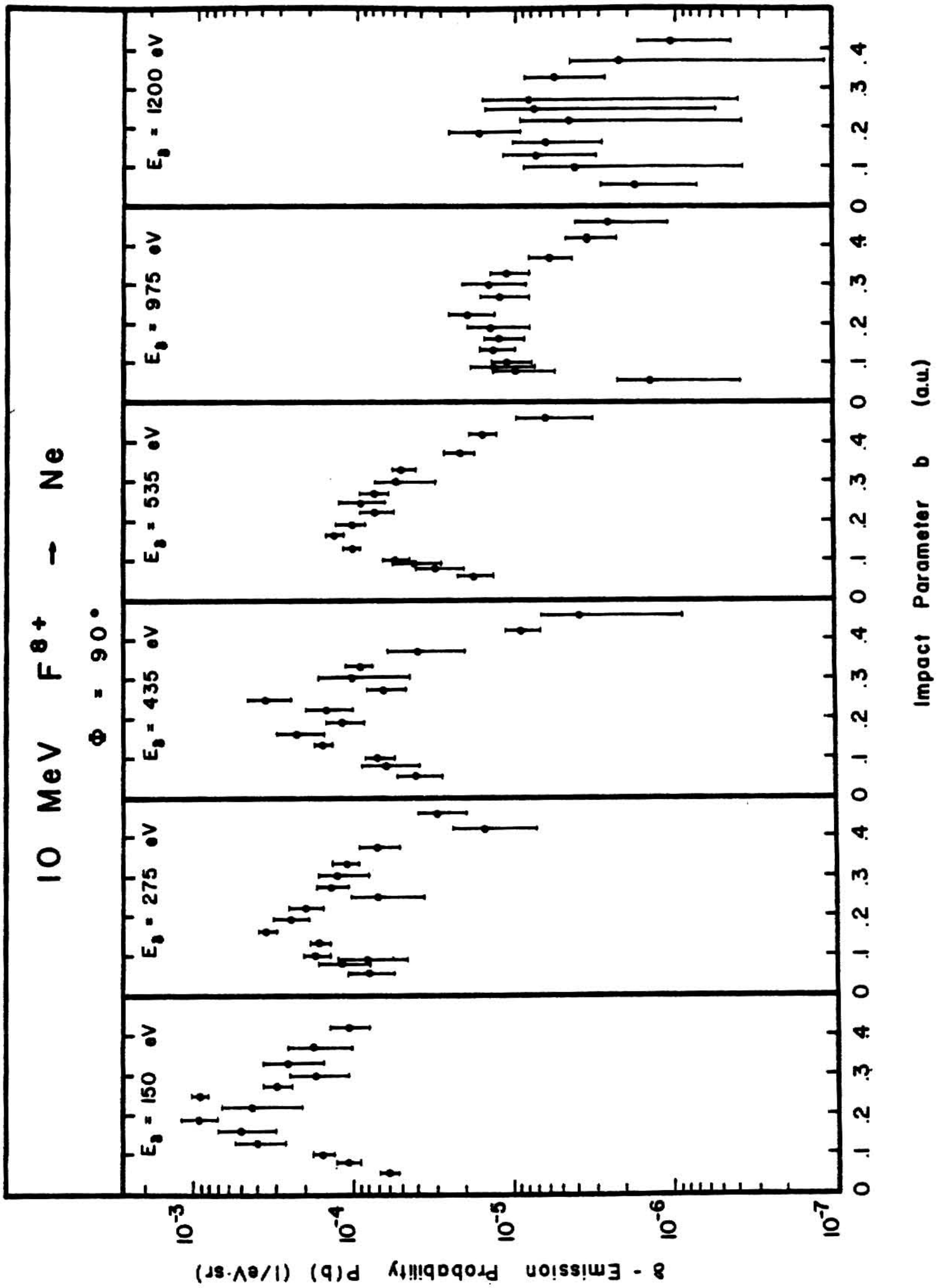
10 MeV F8+ → Ne
Φ = 90°
Eδ = 150 eV
Eδ = 275 eV
Eδ = 435 eV
Eδ = 535 eV
Eδ = 975 eV
Eδ = 1200 eV
Impact Parameter b (a.u.)
δ - Emission Probability P(b) (1/eV-sr)
10-3
10-4
10-5
10-6
10-7
0 .1 .2 .3 .4

Figure 18. Impact parameter dependence of the delta-electron emission probability in 10 MeV F^{9+} + Ne, $\phi = 52.5^{o}$. The impact parameter is subject to an uncertainty of ±5%.

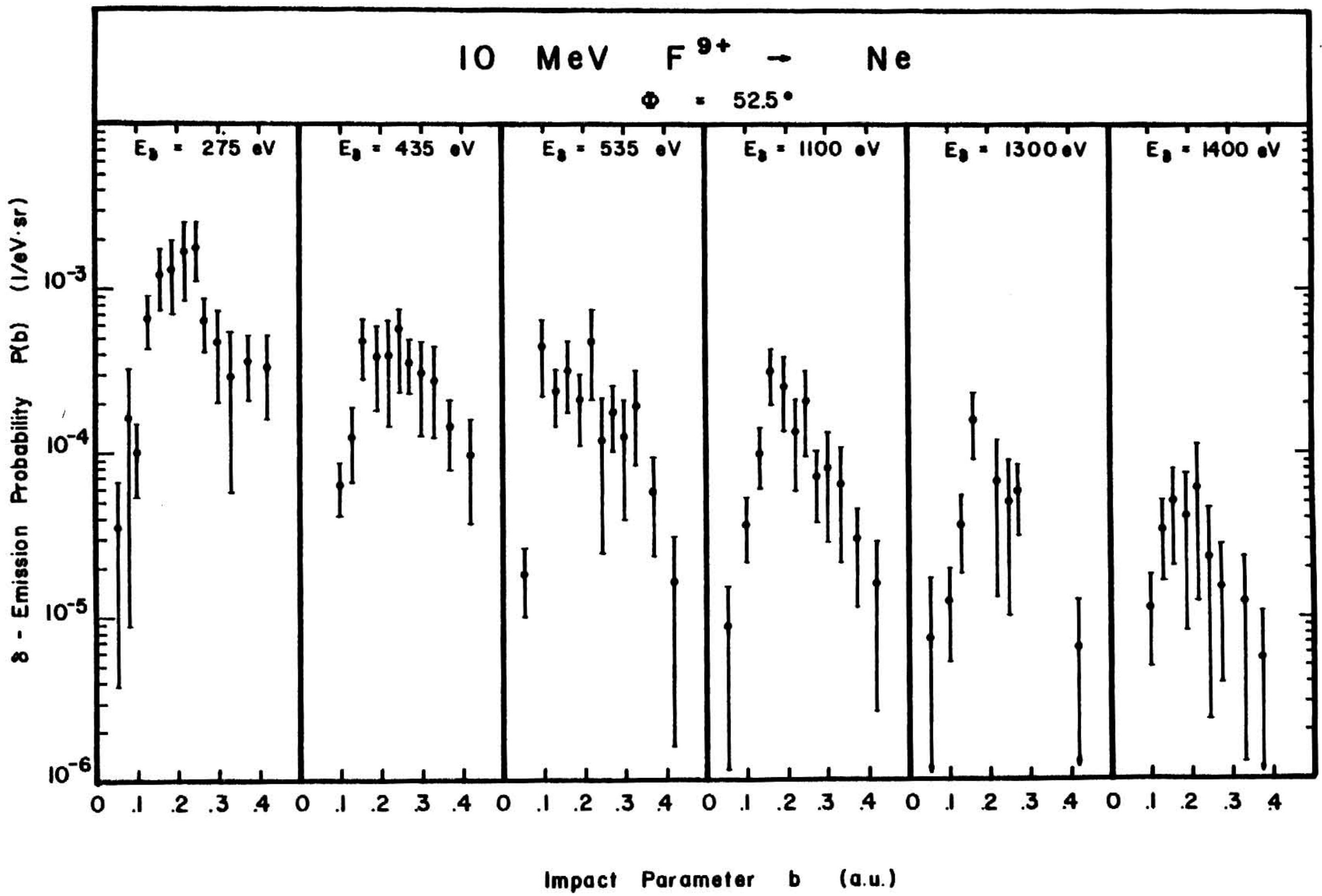

10 MeV F^{9+} → Ne
Φ = 52.5°
$E_δ$ = 275 eV
$E_δ$ = 435 eV
$E_δ$ = 535 eV
$E_δ$ = 1100 eV
$E_δ$ = 1300 eV
$E_δ$ = 1400 eV
δ - Emission Probability P(b) (1/eV·sr)
10^{-3}
10^{-4}
10^{-5}
10^{-6}
0 .1 .2 .3 .4
Impact Parameter b (a.u.)

Figure 19. Impact parameter dependence of the delta-electron emission probability in 10 MeV F^{9+} + Ne, $\phi = 90.0^{o}$. The impact parameter is subject to an uncertainty of ±5%.

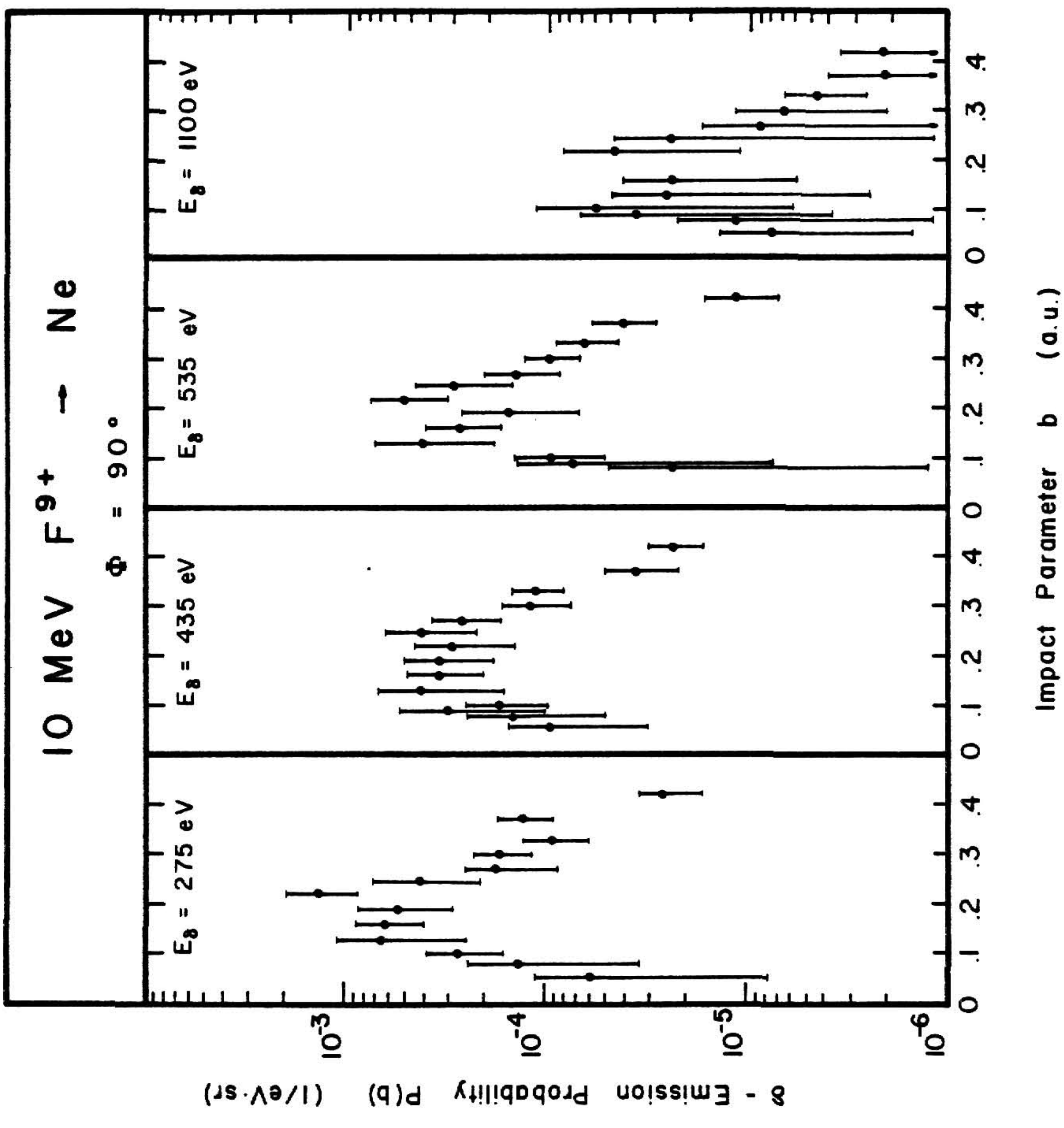
10 MeV F^{9+} → Ne
Φ = 90°
E_δ = 275 eV
E_δ = 435 eV
E_δ = 535 eV
E_δ = 1100 eV
10^{-3}
10^{-4}
10^{-5}
10^{-6}
0 .1 .2 .3 .4
δ - Emission Probability P(b) (1/eV·sr)
Impact Parameter b (a.u.)

Figure 20. Impact parameter dependence of the delta-electron emission probability in 10 MeV F^{9+} + Ne, ϕ =127.5^{o}. The impact parameter is subject to an uncertainty of ±5%.

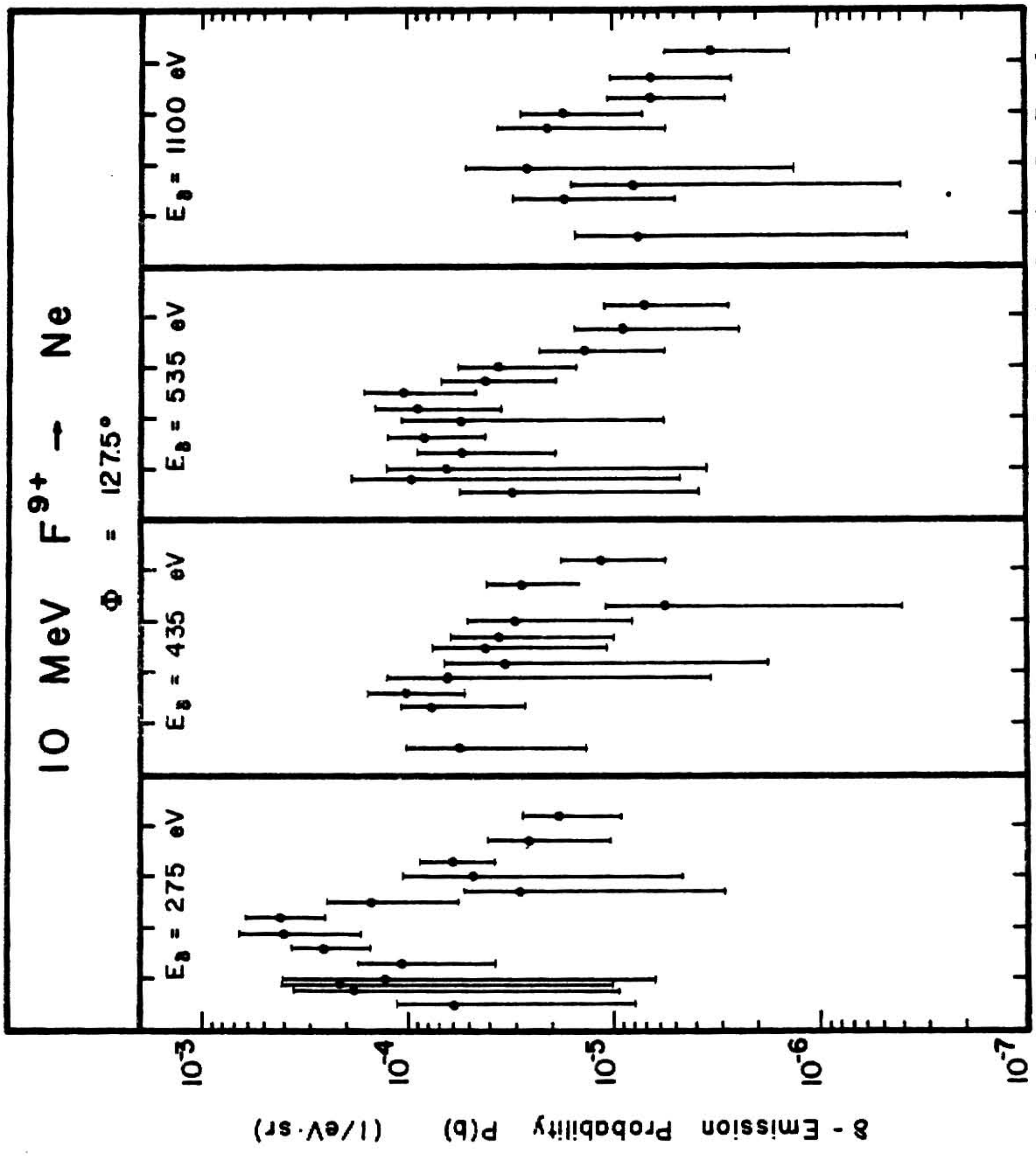

10 MeV F9+ → Ne
Φ = 127.5°
Eδ = 275 eV
Eδ = 435 eV
Eδ = 535 eV
Eδ = 1100 eV
10-3
10-4
10-5
10-6
10-7
δ - Emission Probability P(b) (1/eV·sr)
0 .1 .2 .3 .4
Impact Parameter b (a.u.)

value of the emission probabilities is located at about .15±.02 a.u. and seems (within experimental errors) to shift slightly to smaller impact parameters for decreasing delta-electron energy. The region of maximum emission probability coincides with the adiabatic radius for K-shell electrons of Neon, given by

$$r_{ad}(K) = \frac{\hbar v_p}{E_B(K)} = .146 \text{ a.u.} \tag{5.6}$$

This distance is characteristic for collisions at low velocities and for a Coulombic interaction only. The maximum contribution to the total Coulomb ionization cross section is given for projectiles with an impact parameter b equal to r_{ad}.[25]

In the cases where the effects of projectiles with different charge states on the delta-electron emission probability have been investigated, i.e. in 10 MeV F^{q+} + Ne, q= 6, 8, 9, $\phi = 90^0$, the emission probability does not increase with the number of projectile electrons. The values for P(b) obtained in collisions involving F^{8+} and F^{6+} as projectiles lie between 5% and 10% and between 10% and 15% respectively below those obtained from collisions of F^{9+} with Neon. This again suggests, especially at low delta-electron energies E_δ, that target electrons are the major contributors to the delta-electrons observed at 90^0. This feature confirms the results obtained with DDCS (Section 5-1, ii).

b) Delta-Electron Emission Probabilities as a Function of the Delta-Electron Energy E_δ

For a delta-electron emission angle $\phi = 127.5^0$ and 90^0 the emission probability P(b) falls off exponentially with delta-electron energy E_δ for all observed collision systems and all impact parameters b (see Figures 21 to 23). This energy dependence was already observed in the

Figure 21. Energy dependence of the delta-electron emission probability in 10 MeV F^{6+} + Ne, $\phi = 90.0^o$. The delta-electron energy is subject to an uncertainty of ±40 eV.

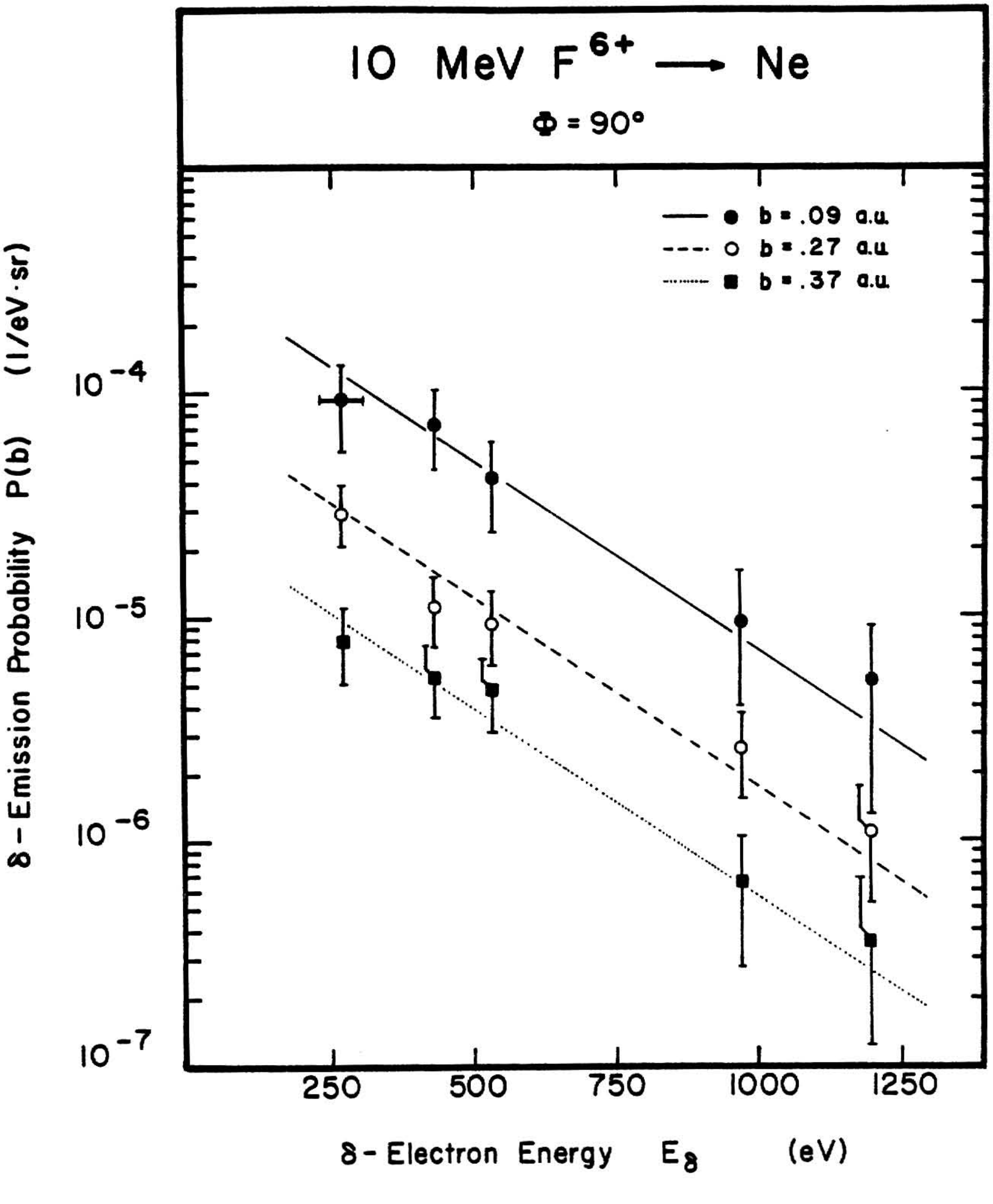
10 MeV F^{6+} → Ne
Φ = 90°
b = .09 a.u.
b = .27 a.u.
b = .37 a.u.
10^{-4}
10^{-5}
10^{-6}
10^{-7}
250
500
750
1000
1250
δ - Emission Probability P(b) (1/eV·sr)
δ - Electron Energy E_δ (eV)

Figure 22. Energy dependence of the delta-electron emission probability in 10 MeV F^{8+} + Ne, $\phi = 90.0^{o}$. The delta-electron energy is subject to an uncertainty of ±40 eV.

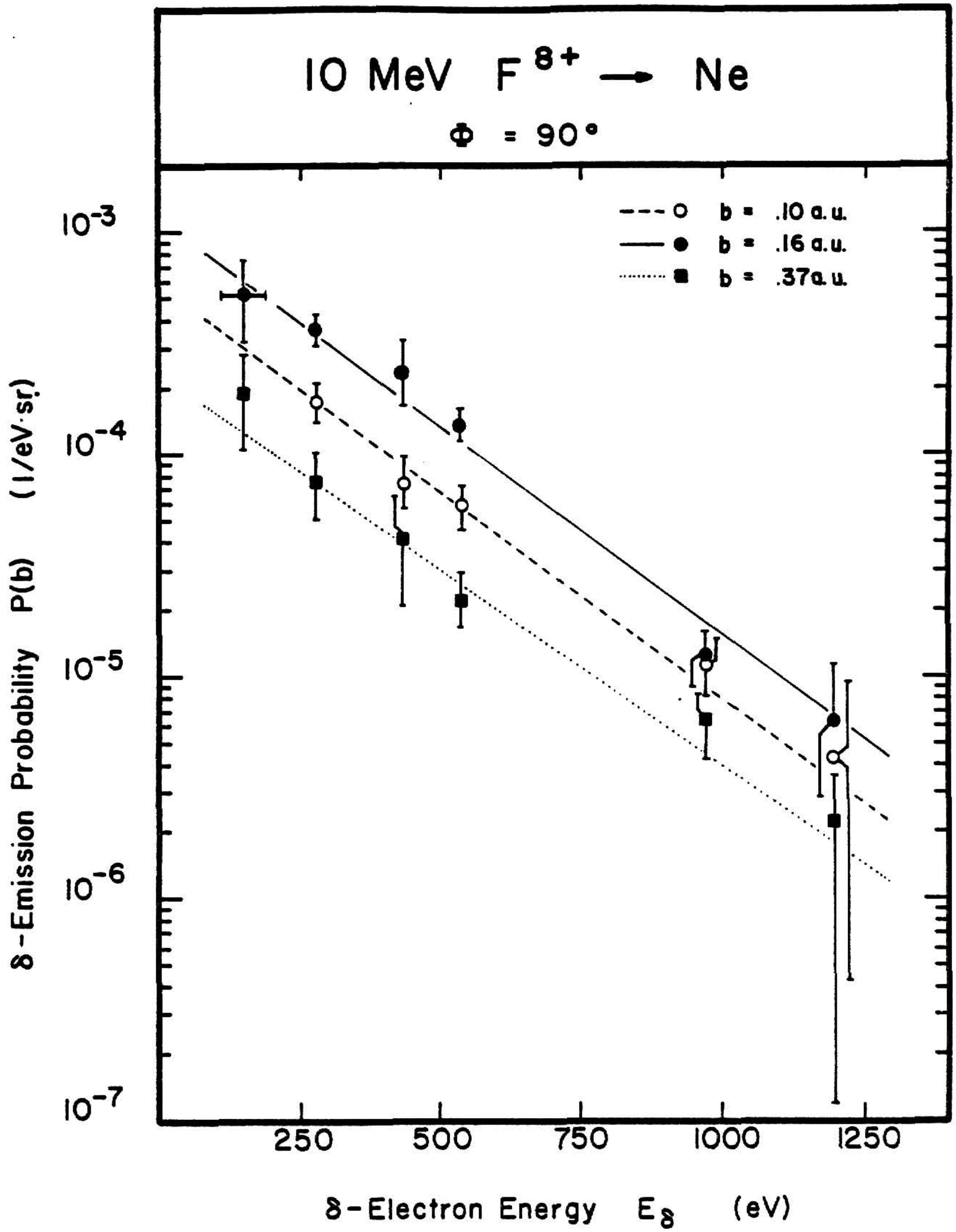

10 MeV F^{8+} → Ne
Φ = 90°
b = .10 a.u.
b = .16 a.u.
b = .37 a.u.
10^{-3}
10^{-4}
10^{-5}
10^{-6}
10^{-7}
δ-Emission Probability P(b) (1/eV·sr)
250
500
750
1000
1250
δ-Electron Energy E_δ (eV)

Figure 23. Energy dependence of the delta-electron emission probability in 10 MeV F^{9+} + Ne, $\phi = 90.0^{\circ}$. The delta-electron energy is subject to an uncertainty of ±40 eV.

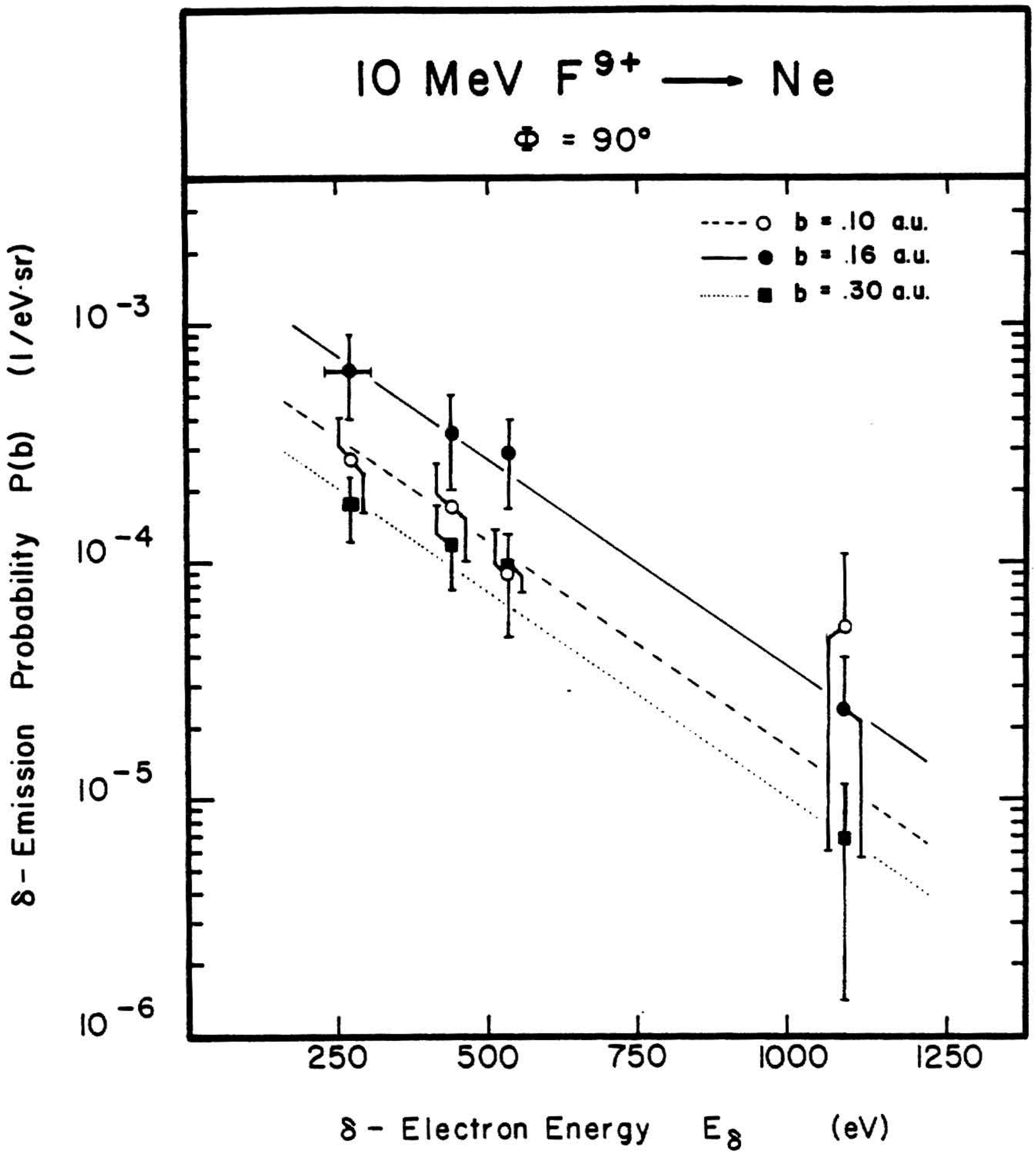
10 MeV F^{9+} ⟶ Ne
Φ = 90°
b = .10 a.u.
b = .16 a.u.
b = .30 a.u.
10^{-3}
10^{-4}
10^{-5}
10^{-6}
δ - Emission Probability P(b) (1/eV·sr)
250
500
750
1000
1250
δ - Electron Energy E_δ (eV)

DDCS (Section 5-1, ii). Within experimental errors the slope of P(b) versus E_δ in a semilogarthimic plot can be chosen to be approximately -.0167 for all investigated collision systems with ϕ = 127.5^o and 90^o.

For the system 10 MeV F^{9+} + Ne, ϕ = 52.5^o (see Figure 24), the emission probability falls off exponentially with approximately the same slope as in the previous cases for delta-electron energies smaller 600 eV. Above this energy the binary encounter peak starts to play a major role. Within the given errors this peak seems to become shallower and less wide for increasing impact parameters, indicating that the "hardness" of the collision with maximum momentum transfer decreases.

c) Delta-Electron Emission Probabilities as a Function of the Delta-Electron Emission Angle ϕ

The angluar dependence of the delta-electron emission probabilities was investigated in the system 10 MeV F^{9+} + Ne, ϕ = 52.5^o, 90^o and 127.5^o with respect to the beam direction.

In Figure 25 the emission probability as a function of E_δ is given for all three emission angles at b = .16 a.u. The probability at ϕ=127.5^o is a factor 3 lower than at 90^o. For E_δ smaller than 600 eV, the probability at ϕ = 52.5^o is a factor 1.5 above the one for ϕ = 90^o. Above this energy the binary encounter peak is the major contributor to P(b) for ϕ = 52.5^o. If the same set of data is presented in a polar diagram (Figure 26), the strong asymmetric distribution of the delta-electron probability in forward beam direction becomes obvious.

5-3) Error Analysis

Due to the construction of the spherical sector spectrometers in use to energy analyze the delta-electrons, the angles at which electrons

Figure 24. Energy dependence of the delta-electron emission probability in 10 MeV F^{9+} + Ne, ϕ =52.5^{o}. The delta-electron energy is subject to an uncertainty of ±40 eV.

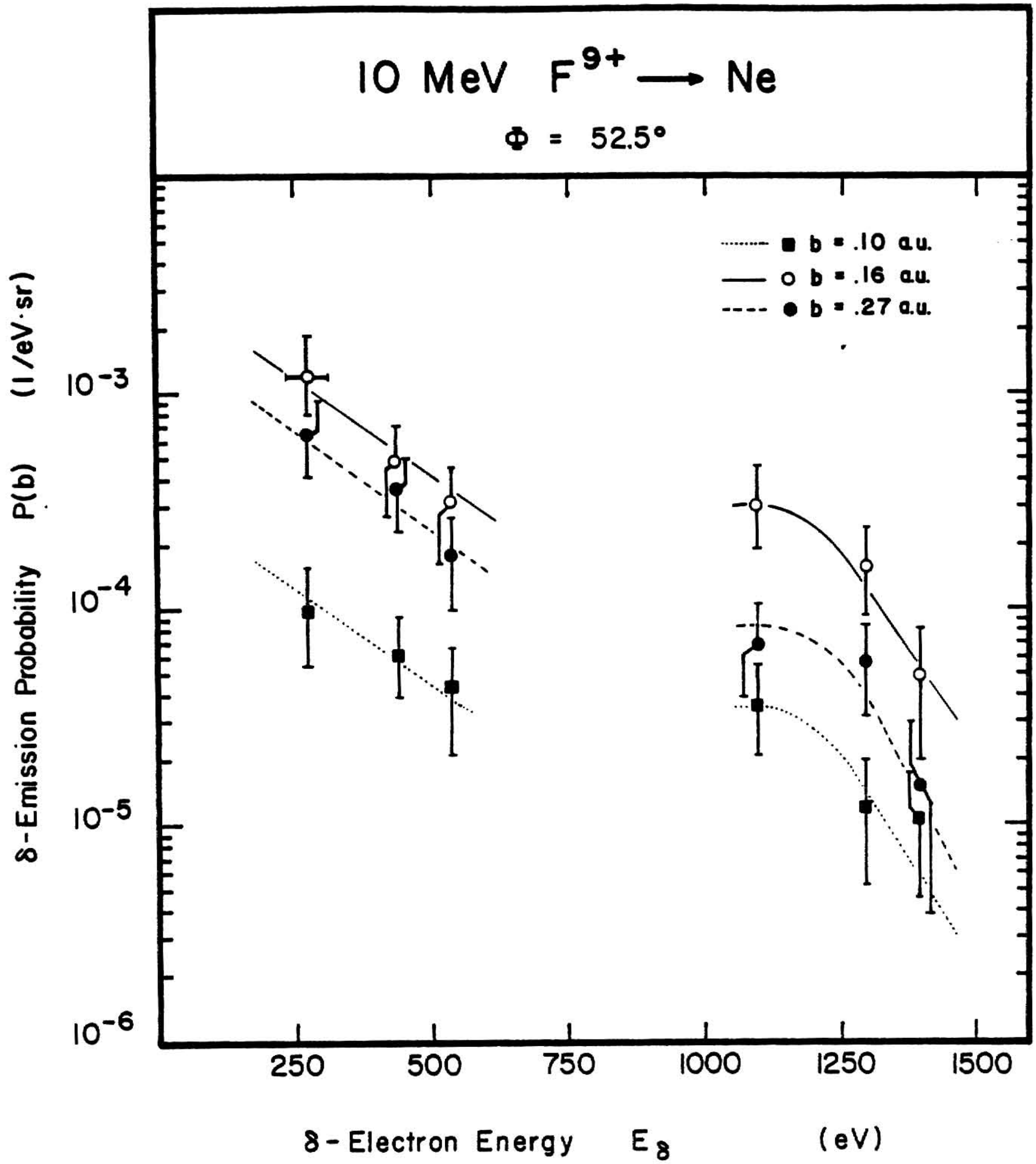
10 MeV $F^{9+} \longrightarrow$ Ne
Φ = 52.5°
b = .10 a.u.
b = .16 a.u.
b = .27 a.u.
δ-Emission Probability P(b) (1/eV·sr)
10^{-3}
10^{-4}
10^{-5}
10^{-6}
250
500
750
1000
1250
1500
δ-Electron Energy E_δ (eV)

Figure 25. Angular dependence of the delta-electron emission probability in 10 MeV F^{9+} + Ne, shown in a plot P(b) vs E_δ for b = .16 a.u.

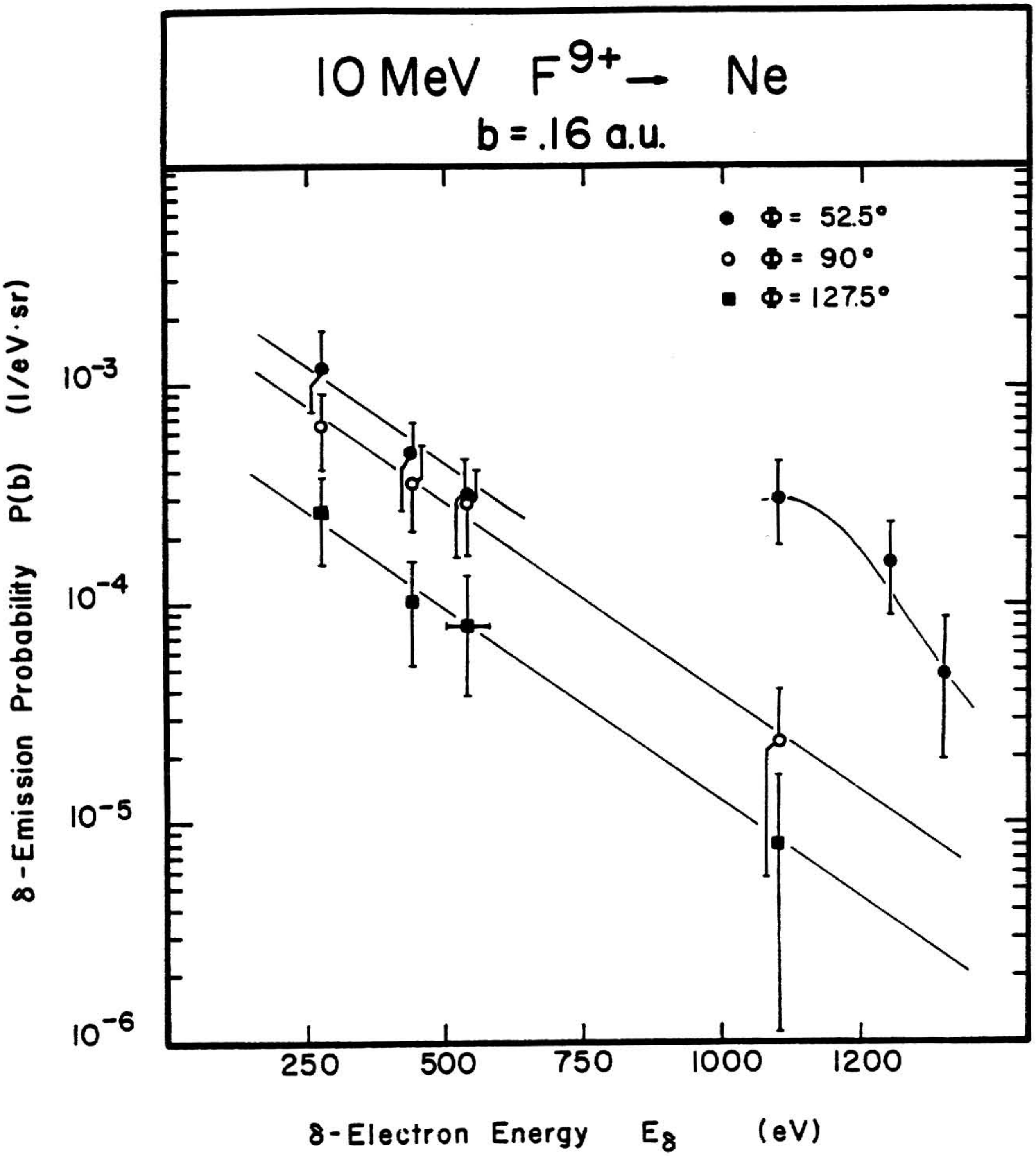
10 MeV $F^{9+} \rightarrow$ Ne
b = .16 a.u.
● Φ = 52.5°
○ Φ = 90°
■ Φ = 127.5°
δ-Emission Probability P(b) (1/eV·sr)
10^{-3}
10^{-4}
10^{-5}
10^{-6}
250
500
750
1000
1200
δ-Electron Energy $E_δ$ (eV)

Figure 26. Polar diagram of the angular dependence of the delta-electron emission probability for b = .16 a.u., E_δ = 275 eV and 1100 eV in 10 MeV F^{9+} + Ne.

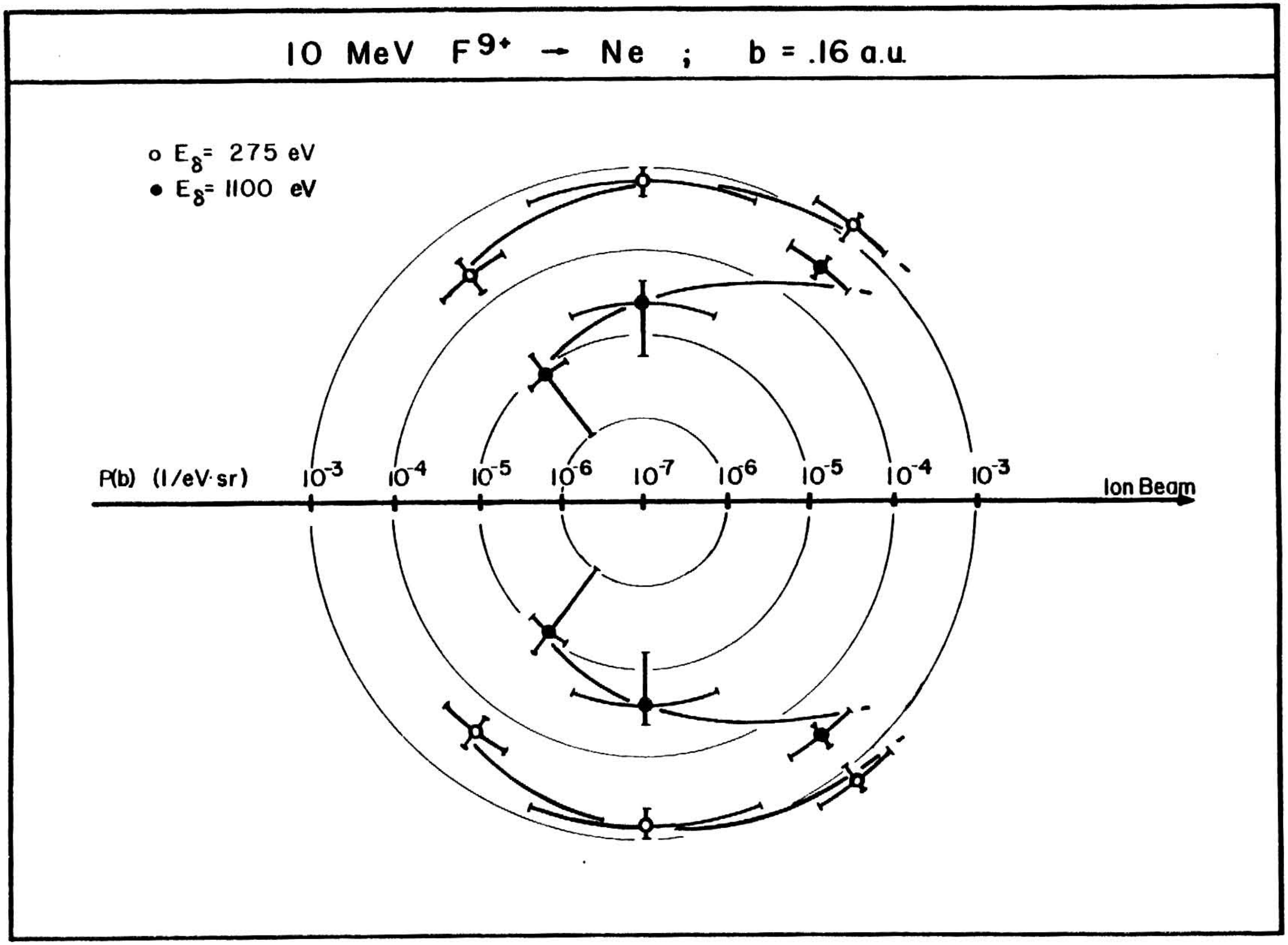

10 MeV F9+ → Ne ; b = .16 a.u.
o Eδ= 275 eV
• Eδ= 1100 eV
P(b) (1/eV·sr)
10-3
10-4
10-5
10-6
10-7
10-6
10-5
10-4
10-3
Ion Beam

can be detected cover a range of $90^o \pm 21^o$, $127.5^o \pm 7.5^o$ and $52.5^o \pm 7.5^o$ with respect to the beam direction (see Chapter 4-2).

The finite size of the collector rings in the Parallel-Plate-Avalanche detector leads to an uncertainty of the impact parameters b of ±5% (see Chapter 4-3).

The energy calibration of the singles electron spectra is accurate within ±2 eV. Due to the sorting and projection process this accuracy is somewhat lessened to within ±6 eV. Since in the course of analyzing the data a window of width 80 eV is chosen to determine the number of coincident delta-electrons (see Chapter 5-2), the uncertainty in delta-electron energy E_δ amounts to ±40 eV. Completely within this margin lies an uncertainty due to the Doppler shift of the electron energy.[56]

The uncertainty in the delta-electron emission probability is given for each data point in Figures 16 to 20. It is due to three main contributions. Due to low coincident count rates the statistical error in the number of coincident delta-electrons is the major factor, followed by the statistical error of the coincident Auger-electrons. The third major source of error is the uncertainty in the Auger-electron production probability used to normalize the data presented in this work. These uncertainties are given by Hagmann et al.[34,46,47] and are directly incorporated into this error analysis.

In the best case (F^{8+} + Ne) the uncertainty in the delta-electron emission probability amounts to about ±20%, in the worst case (F^{9+} + Ne, $\phi = 127.5^o$) it comes close to ±100%.

5-4) The Semiclassical Approximation and Its Comparison to the Experimental Results

The principles of the Semiclassical approximation (SCA) have been discussed briefly in Chapter 2. The more detailed description in this section is based on publications by D. Trautmann and F. Roesel.[31]

The discrepancies between calculations based on the earlier mentioned, simple SCA model and experimental results[31] gave rise to various corrections and modifications in the model which will be mentioned here.

The formulation of the ionization process is described by introducing the quantum mechanical Hamiltonian

$$H = T_p + T_T + T_e + \frac{Z_p Z_T e^2}{R'} - \frac{Z_T e^2}{r} - \frac{Z_p e^2}{r'} \qquad (5.7)$$

where T_p, T_T and T_e are the kinetic energy operators for the projectile, target and electron respectively. The electromagnetic interaction terms are defined by the radius vectors $\vec{R}'$ between projectile and target nuclei, $\vec{r}'$ between projectile nucleus and target electron and $\vec{r}$ between target nucleus and target electron. Introducing the channel Hamiltonians

$$H_i = H_f = T_{kin} + \frac{Z_p Z_T e^2}{R} - \frac{Z_T e^2}{r} \qquad (5.8)$$

H can be written as

$$H = H_i + V_i = H_f + V_f \qquad (5.9)$$

which defines the residual interaction as

$$\Delta V(\vec{r},\vec{R}) = -\frac{Z_p e^2}{|\vec{R} - \frac{m_T}{M}\vec{r}|} + \frac{Z_p Z_T e^2}{|\vec{R} + \frac{m_o}{M}\vec{r}|} - \frac{Z_p Z_T e^2}{R} \qquad (5.10)$$

where $M = m_T + m_o$.

Neglecting the recoil terms (second and third term in 5-10) by assuming $m_T \to \infty$, the residual interaction is approximated by

$$\Delta V(\vec{r},\vec{R}) \simeq -\frac{Z_p e^2}{|\vec{R} - \vec{r}|} \qquad (5.11)$$

which leads back to the model introduced in Chapter 2.

The transition matrix element, using a perturbed stationary state approximation of the wave functions, is given by

$$T_{f,i} = \langle \chi_f \, \zeta_f | \Delta V(r,R) | \chi_i \zeta_i \rangle \tag{5.12}$$

with initial and final projectile wave functions χ_i and χ_f and the bound state and continuum electron wave functions ζ_i and ζ_f.

In the adiabatic limit ($V_e \gg V_p$) one obtains the formalism of the Born-Oppenheimer Approximation, in the sudden limit ($V_p \gg V_e$) the Distorted Wave Born Approximation, which uses ζ_i as a wave function of the unperturbed bound electron, is obtained. Both quantal treatments lead to a closed form of the transition matrix element, but are in general very time consuming to carry out.

Several approximations to the transition matrix can be made:

a) One can approximate the projectile wave function by plane waves (PWBA), which gives good results for total cross sections, but not the details in differential cross sections.[31]

b) The SCA as given in Chapter 2. Using classical trajectories $\vec{R}(t)$, one obtains the ionization probability P(b) under the fundamental condition $Z_p \ll Z_T$.

This simple semiclassical picture in b) can be improved by correcting for the following effects:

i) Distortion of the Classical Coulomb Trajectory

For contributions to the ionization process resulting from large impact parameters the projectiles does no longer feel the target atom as a point charge and its motion will be influenced by the screening of the target electrons. To obtain the trajectories, screened potentials of the form

$$V_s(\vec{R}) = - \frac{Z_p Z_T e^2}{R} \cdot \phi\,(\vec{R}) \tag{5.13}$$

with a screening function $\phi(\vec{R})$ are introduced (see also Chapter 3-1). This effect is generally small and only of some importance in the case of ionization from outer shells.

ii) Recoil Effects

In the simple SCA treatment one assumes that the target has infinite mass which leads to the omission of the the recoil terms in the residual interaction. For a finite target mass one has to include these effects and obtains

$$V(\vec{r},\vec{R}) = -Z_p e^2 \left\{ \frac{1}{|\vec{R} - \frac{m_T}{M}\vec{r}|} - \frac{1}{|\vec{R} + \frac{m_o}{M}\vec{r}|} + \frac{Z_T}{R} \right\} \simeq - \frac{Z_p e^2}{|\vec{R}-\vec{r}|} + \Delta V \quad (5.14)$$

with

$$\Delta V \simeq \frac{Z_p Z_T e^2}{R^3} \cdot \frac{m_o}{m_T} \cdot (\vec{r} \cdot \vec{R}) \quad (5.15)$$

This term ΔV has a strong resemblance to a dipole term. Therefore, the coherent addition of the recoil term to the "normal" dipole term can lead to significant changes in the ionization probability for large impact parameters.

iii) Binding Effects

This correction is due to a radius dependent binding energy E_B.

$$E_B = E_B(\vec{R}) + \Delta E_B(\vec{R}) \quad (5.16)$$

with

$$\Delta E_B(\vec{R}) = \langle \zeta_i(\vec{v}) \, | \frac{Z_p e^2}{|\vec{R}-\vec{r}|} | \, \zeta_i(\vec{v}) \rangle \quad (5.17)$$

The change in binding energy ΔE_B can be more refined by using PSS wave functions instead of the unperturbed electron wave functions.

iv) United Atom Effects

This correction is based on a model introduced by Briggs[57] for near symmetric systems where the SCA model itself cannot be used without questioning its validity. Starting with the ionization amplitude $a_{f,i}$, the final and initial states are chosen to be united atom states centered around the center of charge during the collision. The interaction term will thus contain changes of both potentials from the target and projectile. The ionization amplitude then becomes

$$a_{f,i} = - i/\hbar \int_{-\infty}^{+\infty} e^{i(E_f^{UA} - E_i^{UA})t/\hbar} \langle \psi_f^{UA} | - \frac{Z_p e^2}{|\vec{r}-p\vec{R}|} - \frac{Z_T e^2}{|\vec{r}-q\vec{R}|} | \psi_i^{UA} \rangle dt \quad (5.18)$$

which is a coherent supperposition of two SCA-type amplitudes with scaled trajectories $p\vec{R}$ and $q\vec{R}$, where

$$p = \frac{Z_p}{Z_p+Z_T} \; ; \; q = 1-p \quad (5.19)$$

Including this effect lowers in general the ionization probability in near symmetric collisions (for 10 MeV F^{9+} + Ne, for the Neon K-shell P(b) is lowered by a factor of 2 to 4, the influence on the L-shell ionization is not yet known[58]).

The only available set of theoretical values to be compared with the experimentally obtained data of the present work is a SCA calculation performed by D. Trautmann.[58] Delta-electron emission probabilities as a function of the impact parameter b, the delta-electron energy E_δ and the delta-electron emission angle ϕ, are obtained for the K-shell and all L-subshells of Neon for impinging 10 MeV F^{9+} with $\phi = 90^o$ by using relativistic hydrogenic wave functions, hyperbolic trajectories and binding corrections. Terms with angular momentum up to ℓ=2 are used in expanding

$$\frac{1}{|\vec{r}-\vec{R}|} = \sum_{\ell} \frac{1}{r^{\ell+1}} \cdot G_\ell(R) \quad (5.20)$$

Figure 27. Comparison of theoretical (SCA) and experimental values of the impact parameter dependence of the delta-electron emission probability in 10 MeV F^{9+} + Ne, ϕ = 90.0^{o}. The theoretical values are given for the K-shell, all L-subshells and as total probabilities and are subject to an uncertainty of ±20%.

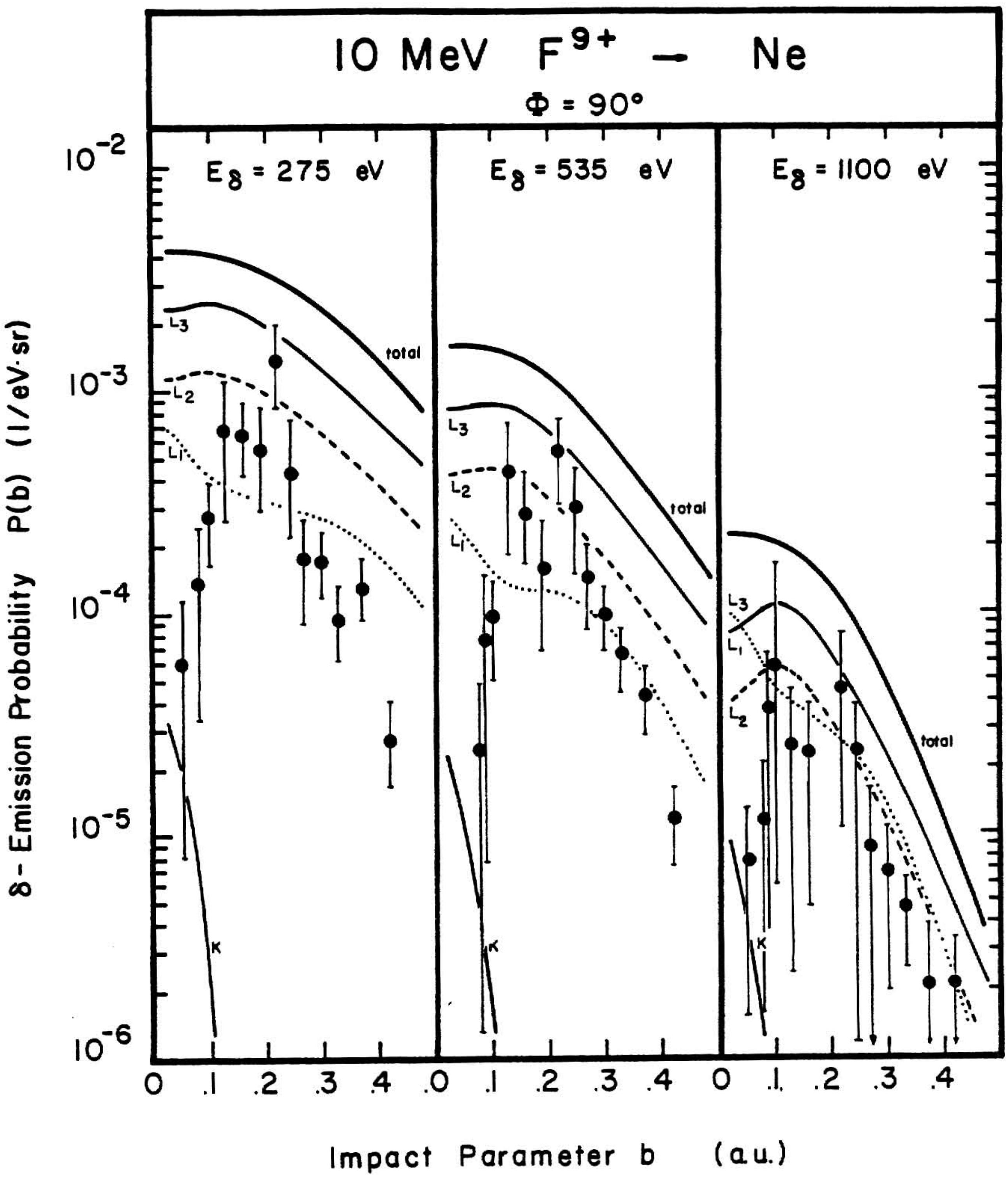
10 MeV F^{9+} → Ne
Φ = 90°
E_δ = 275 eV
E_δ = 535 eV
E_δ = 1100 eV
total
L_3
L_2
L_1
K
10^{-2}
10^{-3}
10^{-4}
10^{-5}
10^{-6}
δ - Emission Probability P(b) (1/eV·sr)
0 .1 .2 .3 .4
Impact Parameter b (a.u.)

Figure 28. Comparison of theoretical (SCA) and experimental values of the impact parameter dependence of the delta-electron emission probability in 10 MeV F^{9+} + Ne, $\phi = 90.0^{o}$. The theoretical values are subject to an uncertainty of ±20%.

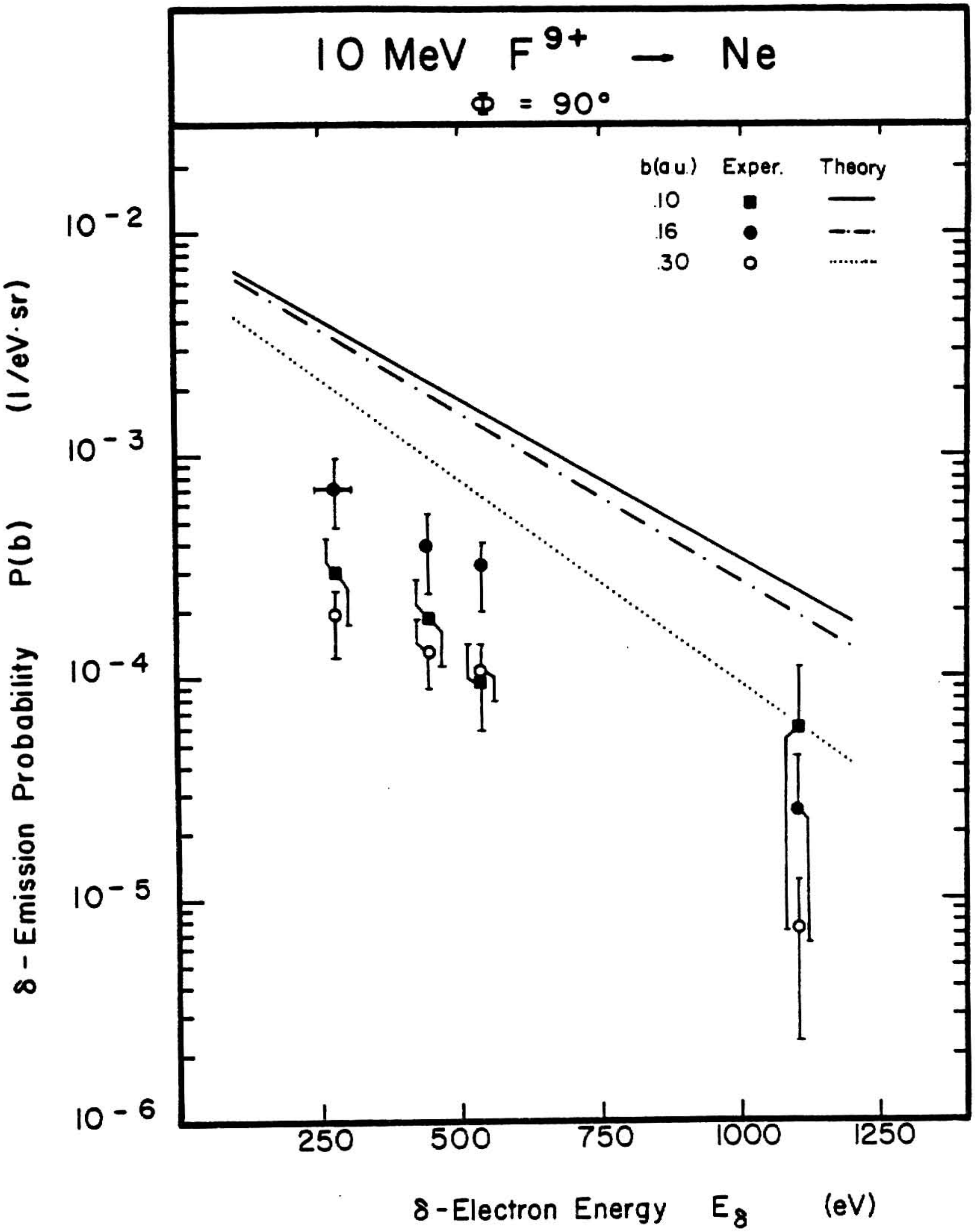
10 MeV F^{9+} → Ne
$\Phi = 90°$
b(a.u.) Exper. Theory
.10
.16
.30
10^{-2}
10^{-3}
10^{-4}
10^{-5}
10^{-6}
δ - Emission Probability P(b) (1/eV·sr)
250
500
750
1000
1250
δ-Electron Energy E_δ (eV)

where G_ℓ contains a polynomial in R and a set of spherical harmonics. These theoretical values are subject to an uncertainty of 20%. They are tabulated in Appendix 1 and compared to the experimental data set in Figures 27 and 28.

As can be seen in Figure 28, the electron energy dependence is followed by the experimental values within the given uncertainties. However, neither the shape nor the magnitude of P(b) as a function of b are reproduced correctly (Figure 27). The theoretical curve is on the order of one magnitude above the experimental results and the rapid drop of P(b) for decreasing impact parameters inside .15 a.u. is not given. Since this drop was observed previously,[11] the validity of calculations within an SCA-type picture for near symmetric collision systems is doubtful. However, the incorporation of the united-atom correction and the use of Hartree-Fock wave functions might reduce the discrepancy between experimental and theoretical values.[58] Such calculations will be available in the near future.

Chapter 6

CONCLUSION

The absolute triple differential probabilities for delta-electron emission in 10 MeV F^{q+} + Ne (q = 6, 8, 9) have been measured as a function of the impact paramter, the delta-electron energy and the delta-electron emission angle. The probabilities show a strong asymmetry in forward beam direction due to electrons originating in hard collisions with maximum momentum transfer to the electron (binary encounter peak). For lower delta-electron energies the energy dependence of the ionization probabilities takes an approximately exponentially decaying shape due to the momentum distribution of the target electrons originating in soft collisions with minimum momentum transfer to the electron. The impact parameter dependence of the probabilities show a strong peak at an impact parameter of about 1.5 times the K-shell radius (.38 times the L-shell radius) of Neon. A steep rise to this maximum, previously observed by Cocke et al.,[11] was also found in this collision system.

Further experiments to clarify the direct ionization process in heavy ion-atom collisions are necessary. Among them are coincidence measurements between delta-electrons and charge-state analyzed recoil ions and triple coincidence measurements between delta-electrons, scattered particles and recoil ions. The not well understood steep rise of P(b) to its maximum for increasing impact parameters might be due to a dominant capture process of the Neon L-shell electrons by the projectile. An experiment measuring the charge state and scattering angle of the projectiles coincident with delta- and Auger-electrons could clarify this process.

A comparison with a theoretical calculation based on the framework of the SCA reproduces the energy dependence of the delta-electron emission probabilties, but show large discrepancies in the impact parameter dependence and in the magnitude of the probabilities. The stationary position of the peak in P(b) as a function of b in all investigated cases is not understood.

Further improvements of theoretical models, especially their extensions into the region of this experimental collision system where neither adiabatic nor sudden limit arguments are valid, are highly desirable.

REFERENCES

1. L. H. Toburen, Phys. Rev. A9, 2505 (1974).
2. Y.-K. Kim, Radiat. Res. 64, 96 (1975).
3. M. E. Rudd, Radiat. Res. 64, 153 (1975).
4. Y.-K. Kim, Radiat. Res. 64, 205 (1975).
5. M. E. Rudd, L. H. Toburen and N. Stolterfoht, At. Data Nuc. Data Tables 18, 413 (1976).
6. T. L. Criswell, L. H. Toburen and M. E. Rudd, Phys. Rev. A16, 508 (1977).
7. L. H. Toburen, S. T. Manson and Y.-K. Kim, Phys. Rev. A17, 148 (1978).
8. S. T. Manson and L. H. Torburen, Phys. Rev. Lett. 46, 529 (1981).
9. F. Bell, G. Trollmann, H. Boeckl, J. Phys. B15, 1487 (1982).
10. T. H. Weiter and R. Schuch, Z. Phys. A305, 91 (1982).
11. C. L. Cocke, H. Schmidt-Boecking and R. Schuch, J. Phys. B15, 651 (1982).
12. J. H. Miller, L. H. Toburen and S. T. Manson, Phys. Rev. A27, 1337 (1983).
13. W. Brandt, Proc. 3rd Int. Conf. Atom. Phys., Boulder, Colorado (1972), ed. S. J. Smith (Plenum Press, New York).
14. W. Brandt, Proc. Int. Conf. on Inner-Shell Ionization Phenomena, Atlanta Georgia, 1972, ed. R. Fink (North-Holland, Amsterdam).
15. E. Merzbacher and H. L. Lewis, in "Handbuch der Physik", Vol. XXXIV, p. 166, 1958, ed. S. Fluegge (Springer, Berlin).
16. G. S. Khandelwal, B. H. Choi and E. Merzbacher, At. Data 1, 103 (1969).
17. B. C. Choi, E. Merzbacher and G. S. Khandelwal, At. Data 5, 291 (1973).

18. G. Basbas, W. Brandt and R. Laubert, Phys. Rev. A7, 983 (1973).

19. J. D. Garcia, R. F. Fortner and T. M. Kavanagh, Rev. Mod. Phys. 45, 111 (1973).

20. J. S. Hansen, Phys. Rev. A7, 822 (1973).

21. J. H. McGuire and P. Richard, Phys. Rev. A8, 1374 (1973).

22. M. Gryzinski, Phys. Rev. 138, A305 (1965); M. Gryzinski, Phys. Rev. 138, A322 (1965); M. Gryzinski, Phys. Rev. 138, A336 (1965).

23. J. Bang and J. M. Hansteen, Kgl. Dan. Vidensk. Selsk. Mat. Fys. Medd. 31, No. 13 (1959).

24. J. M. Hansteen, O. M. Johnson and L. Kocbach, At. Data and Nuc. Data Tables 15, 305 (1975).

25. J. M. Hansteen, Adv. Atom. Mol. Phys. 11, 299 (1975).

26. O. Aashamar and L. Kocbach, Z. Phys. A279, 237 (1976).

27. L. Kocbach, Z. Phys. A279, 233 (1976).

28. L. Kocbach, J. Phys. B9, 2269 (1976).

29. P. A. Amundson, J. Phys. B9, 971 (1976).

30. P. A. Amundson, J. Phys. B10, 1097 (1977).

31. D. Trautmann and F. Roesel, Nuc. Instr. and Meth. 169, 259 (1980).

32. J. M. McGuire, Phys. Rev. A9, 286 (1974).

33. R. Randall, Ph.D. Dissertation, Kansas State University, 1976, unpublished.

34. S. Hagmann, C. L. Cocke, J. R. Macdonald, P. Richard, H. Schmidt-Boecking and R. Schuch, Phys. Rev. A25, 1918 (1982).

35. C. L. Cocke in "Methods of Experimental Physics" Vol. 17, p. 311, 1980, ed. P. Richard, (Academic Press, New York).

36. L. Sarkadi, J. Bossler, R. Hippler and H. O. Lutz, J. Phys. B16, 71 (1983).

37. R. Herzog, J. Phys. 97, 596 (1935).; R. Herzog, Phys. Zeitschr. 41, (1940).

38. W. Schmidt, Diplom Thesis, Universitaet Muenster, W. Germany, 1971, unpublished.

39. W. Schmitz, Ph.D. Dissertation, Universitaet Freiburg, W. Germany, 1976, unpublished.

40. G. Gaukler, H. Schmidt-Boecking, R. Schuch, R. Schule, H. J. Specht and I. Tserruya, Nuc. Instr. and Meth. 141, 115 (1977).

41. W. Brandt, K. W. Jones and H. W. Kramer, Phys. Rev. Lett. 30, 351 (1973).

42. C. L. Cocke and R. Randall, Phys. Rev. Lett. 30, 106 (1973).

43. E. Laegsgaard, J. U. Anderson and L. C. Feldmann, Phys. Rev. Lett. 29, 1206 (1972).

44. K. E. Stiebing, H. Schmidt-Boecking, R. Schule, K. Bethge and I. Tserruya, Phys. Rev. A14, 146 (1976).

45. H. Raether, in "Electron Avalanches and Breakdown in Gases", 1964 (Butterworths, London).

46. S. Hagmann, C. L. Cocke, P. Richard, H. Schmidt-Boecking and R. Schuch, III. Winterschool on Energetic Atomic Collisions, Schoenau, West Germany, January 1982.

47. S. Hagmann, C. L. Cocke, P. Richard, A. Skutlartz, H. Schmidt-Boecking and R. Schuch, Int. Conf. on X-Ray and Atomic Inner-Shell Physics, Eugene, Oregon, August 1982.

48. C. Woods, R. Kauffmann, K. Jamison, N. Stolterfoht and P. Richard, J. Phys. B8, L61 (1975).

49. E. Weigold, Aust. J. Phys. 35, 571 (1982).

50. I. E. McCarthy and E. Weigold, Am. J. Phys. 51, 152 (1983).

51. M. Stoeckli, Kansas State University, private communication.

52. J. D. Garcia, Phys. Rev. 177, 223 (1969).

53. M. E. Rudd, Phys. Rev. A20, 787 (1979).

54. K. Taulbjerg, J. S. Briggs and J. Vaaben, J. Phys. B9, 1351 (1976).

55. W. E. Meyerhof, Phys. Rev. Lett. 31, 1341 (1973).

56. P. Dahl, M. Rodbro, B. Fastrup and M. E. Rudd, J. Phys. B9, 1567 (1976).

57. J. S. Briggs, J. Phys. B8, L485 (1975).

58. D. Trautmann, Universitaet Basel, Switzerland, private communication.

APPENDIX 1

SCA - calculation by D. Trautmann, Universitaet Basel, Switzerland, for the system

10 MeV F^{9+} + Ne, $\phi = 90^{o}$ (Ref. 58)

Delta-Electron Emission Probabilities P(b) in (1/MeV·sr)

E_{δ} = 100 eV

b (a.u.)	K-shell	L_1-shell	L_2-shell	L_3-shell	Total
.450	.247 E-7	.341 E3	.629 E3	.228 E4	.325 E4
.340	.140 E-4	.454 E3	.160 E4	.215 E4	.366 E4
.270	.596 E-3	.505 E3	.139 E4	.280 E4	.470 E4
.180	.474 E-1	.700 E3	.182 E4	.366 E4	.618 E4
.135	.595 E0	.881 E3	.194 E4	.388 E4	.670 E4
.108	.201 E1	.103 E4	.195 E4	.390 E4	.688 E4
.054	.179 E2	.142 E4	.189 E4	.377 E4	.710 E4
.036	.327 E2	.144 Ef	.186 E4	.371 E4	.715 E4
.027	.423 E2	.161 E4	.185 E4	.369 E4	.719 E4

E_δ = 250 eV

b (a.u.)	K-shell	L_1-shell	L_2-shell	L_3-shell	Total
.450	.811 E-8	.134 E3	.278 E3	.566 E3	.968 E3
.340	.669 E-5	.234 E3	.530 E3	.106 E4	.183 E4
.270	.323 E-3	.280 E3	.745 E3	.149 E4	.252 E4
.180	.418 E-1	.326 E3	.108 E4	.216 E4	.357 E4
.135	.391 E0	.362 E3	.119 E4	.238 E4	.394 E4
.108	.136 E1	.407 E3	.122 E4	.243 E4	.405 E4
.054	.133 E2	.580 E3	.119 E4	.238 E4	.416 E4
.036	.252 E2	.653 E3	.118 E4	.235 E4	.420 E4
.027	.331 E2	.686 E3	.117 E4	.234 E4	.423 E4

E_δ = 550 eV

b (a.u.)	K-shell	L_1-shell	L_2-shell	L_3-shell	Total
.450	.117 E-8	.214 E2	.540 E2	.108 E3	.183 E3
.340	.153 E-5	.672 E3	.134 E3	.268 E3	.469 E3
.270	.951 E-4	.107 E3	.214 E3	.428 E3	.739 E3
.180	.165 E-1	.129 E3	.366 E3	.732 E3	.123 E4
.135	.177 E0	.127 E3	.425 E3	.850 E3	.140 E4
.108	.672 E0	.136 E3	.440 E3	.881 E3	.146 E4
.054	.777 E1	.204 E3	.431 E3	.862 E3	.150 E4
.036	.156 E2	.238 E3	.423 E3	.847 E3	.152 E4
.027	.211 E2	.255 E3	.421 E3	.841 E3	.153 E4

E_δ = 850 eV

b (a.u.)	K-shell	L_1-shell	L_2-shell	L_3-shell	Total
.450	.199 E-9	.370 E1	.100 E2	.201 E2	.388 E2
.340	.340 E-6	.216 E2	.322 E2	.644 E2	.188 E3
.270	.279 E-4	.451 E2	.595 E2	.119 E3	.224 E3
.180	.665 E-2	.690 E2	.123 E3	.245 E3	.437 E3
.135	.816 E-1	.746 E2	.150 E3	.300 E3	.525 E3
.108	.337 E0	.837 E2	.157 E3	.314 E3	.556 E3
.054	.446 E1	.123 E3	.149 E3	.298 E3	.584 E3
.036	.997 E1	.155 E3	.144 E3	.188 E3	.597 E3
.027	.139 E2	.166 E3	.142 E3	.283 E3	.605 E3

E_δ = 1150 eV

b (a.u.)	K-shell	L_1-shell	L_2-shell	L_3-shell	Total
.450	.179 E-10	.743 E0	.170 E1	.341 E1	.585 E1
.340	.751 E-7	.726 E1	.690 E1	.138 E2	.280 E2
.270	.815 E-5	.179 E2	.151 E2	.302 E2	.632 E2
.180	.268 E-2	.319 E2	.394 E2	.787 E2	.150 E3
.135	.381 E-1	.376 E2	.515 E2	.103 E3	.192 E3
.108	.172 E0	.444 E2	.545 E2	.109 E3	.208 E3
.054	.285 E1	.750 E2	.469 E2	.930 E2	.220 E3
.036	.648 E1	.891 E2	.423 E2	.845 E2	.222 E3
.027	.926 E1	.959 E2	.404 E2	.808 E2	.220 E3

APPENDIX 2

Impact parameter dependence for Neon K-Auger satellite and hypersatellite production for Fluorine impact at 10 MeV

a) 10 MeV F^{6+} + Ne (Ref. 34)

Neon K-Auger Satellites

b (a.u.)	P(b)	b (a.u.)	P(b)
.420	.008	.190	.200
.370	.023	.160	.263
.330	.035	.130	.273
.300	.055	.100	.234
.270	.078	.090	.218
.245	.108	.080	.206
.220	.140	.055	.170

b) 10 MeV F^{8+} + Ne (Ref. 34)

Neon K-Auger Satellites

b (a.u.)	P(b)	b (a.u.)	P(b)
.460	.130	.190	.750
.420	.200	.160	.575
.370	.370	.130	.370
.330	.520	.100	.200
.300	.650	.090	.160
.270	.760	.080	.120
.245	.830	.055	.070
.220	.850		

c) 10 MeV F^{9+} + Ne (Ref. 46, 47)

Neon K-Auger Satellites

b (a.u.)	P(b)	b (a.u.)	P(b)
.420	.113	.190	.545
.370	.187	.160	.374
.330	.253	.130	.226
.300	.320	.100	.148
.270	.408	.090	.126
.245	.500	.080	.108
.220	.653	.055	.070

DELTA-ELECTRON EMISSION
IN 10 MeV F^{q+} + Ne (q = 6,8,9)

by

ALEXANDER ERICH SKUTLARTZ

Staatsexamen, Universitaet Freiburg, West Germany, 1980

AN ABSTRACT OF A MASTER'S THESIS

submitted in partial fulfillment of the

requirements for the degree

MASTER OF SCIENCE

Department of Physics

KANSAS STATE UNIVERSITY
Manhattan, Kansas

1983

Absolute triple differential probabilities for the ionization of delta-electrons in the near symmetric collision system 10 MeV F^{q+} + Ne, for q = 6,8,9, as a function of delta-electron energy, delta-electron emission angle and impact parameter have been measured.

The probabilities feature a strong asymmetry in forward beam direction due to electrons originating in hard collisions with maximum momentum transfer to the electron. The energy dependence of the emission probabilities follows an exponentially decaying curve for lower delta-electron energies. This form stems from the momentum distribution of the target electrons ionized in soft collisions with minimum momentum transfer to the electron. The probabilities show a strong peak at an impact parameter of 1.5 times the K-shell radius of Neon. They rise very sharply to this maximum for increasing impact parameters and fall off exponentially after reaching the peak.

The experimentally obtained data are compared to a theoretical calculation based on the Semiclassical Approximation. Large discrepancies exist in the magnitude of the probabilities and their impact parameter dependence, but the energy dependence is reproduced by the theoretical model.